TABLE I
Experimental restraints and structural statistics of final 20 structures

Total number of distance restraints	1630
Intraresidue ($\|i - j\| = 0$)	639
Sequential ($\|i - j\| = 1$)	372
Medium range ($1 < \|i - j\| < 5$)	211
Intramolecular long range ($\|i - j\| \geq 5$)	305
Intermolecular	103
Number of hydrogen bonds	25
Number of dihedral angle restraints	50
Energies[a]	
Mean AMBER energy (kcal/mol)	−5172 ± 14
Mean van der Waals' energy (kcal/mol)	−937 ± 12
Mean constraint energy (kcal/mol)	18 ± 1
Mean deviations from ideal geometry	
Bond lengths (Å)	0.0100 ± 0.0001
Bond angles (°)	2.31 ± 0.01
Violation statistics	
Number of distance violation > 0.2 Å	0.6 ± 0.5
Maximum distance violation (Å)	0.27
Number of dihedral angle violation > 2°	0.3 ± 0.4
Maximum dihedral angle violation (°)	3.64
Root mean square deviation from the average structure*	
Backbone (Å)	0.34 ± 0.06
Heavy atoms (Å)	0.78 ± 0.06
PROCHECK statistics[b]	
Residues in most favoured regions (%)	91.4
Residues in allowed regions (%)	7.9
Residues in generously allowed regions (%)	0.6
Residues in disallowed regions (%)	0.1

[a] Generalized Born model of AMBER 7 was used.
[b] Residues 1–75 of HR23B and 278–296 of S5a were used.

Met^{73} of the UbL β-sheet; the side chains of these residues form a pocket that packs tightly around the methyl group of Ala^{290} of UIM (Fig. 3, *b* and *c*). Leu^{8} also forms hydrophobic interactions with Leu^{278} of UIM. Mutation of Leu^{8} or Val^{71} of UbL or of Ala^{290} of UIM largely abolishes binding, indicating that the surface complementarity of these residues is important for binding (Table II).

The association of the UIM helix is further stabilized by two polar interactions near both of its ends. Ser^{294} of UIM accepts a hydrogen bond from the main chain amide group of Gly^{50} of UbL, which adopts a consecutive type IV (residues 47–50) and type I′ (residues 48–51) β-turns (β_T; Fig. 3, *b* and *c*). This conformation, which is stabilized by an aromatic-methyl stacking interaction between the phenol ring of Tyr^{48} and the methyl group of Ala^{49}, places the amide group of Gly^{50} in a suitable position to form an intermolecular hydrogen bond. The significance of this bond can be seen by the total loss of binding that occurs when the hydroxyl group of Ser^{294} is replaced by a proton through a serine-to-alanine mutation (Table II).

The other polar interaction engages Glu^{283}, the N-terminal residue of the UIM helix, whose side chain carboxyl group can be in a position to make an electrostatic interaction with the side chain amino group of Lys-45 of UbL (Fig. 3*b*). Alanine substitution of Glu^{283} moderately decreases binding, suggesting that this charge complementarity is important for binding (Table II).

Comparison of UIM-binding Sites between UbL and Ubiquitin—Interestingly, all of the major UIM contact sites in UbL are conserved in ubiquitin. Residues Leu^{8}, Ile^{44}, Val^{70}, and His^{68} of ubiquitin create a hydrophobic surface that resembles the hydrophobic contact site on UbL (Fig. 3*d*). Previous mutational analyses have shown that, except for His^{68}, these ubiquitin residues are critical for proteasomal degradation and for binding to S5a and are essential for life in yeast (28, 41, 42).

The polar contact sites in UbL are also conserved in ubiquitin. The Phe^{45}-Ala^{46}-Gly^{47} segment of ubiquitin adopts a consecutive type IV (residues 44–47) and type I′ (residues 45–48) β-turns identical to that seen in the Tyr^{48}-Ala^{49}-Gly^{50} segment of UbL with an root mean square deviation of 0.12 Å across the main chain heavy atoms. Thus, the amide group of Gly^{47} of ubiquitin is in the same position as Gly^{50} of UbL, which forms a key hydrogen bond with Ser^{294} of UIM in the complex.

Finally, the positively charged side chain of Arg^{42} in ubiquitin is located in the same position as that of Lys^{45} of UbL and thus possibly mediates an electrostatic interaction with the conserved acidic residue at position 283 of UIM (Fig. 3*d*). Arg^{42} of ubiquitin has been shown to be essential for yeast viability (42).

The striking conservation of UIM-binding sites between ubiquitin and UbL suggests that the contact sites and mode of ubiquitin binding to UIM are similar to those observed in our structure. We confirmed that the effects of mutations in UIM are similar for UIM binding to UbL and UIM binding to tetraubiquitin; in other words, mutating Glu^{283}, Ala^{290}, or Ser^{294} in UIM impairs its binding to tetraubiquitin (Fig. 4). The importance of Ser^{294} of UIM was also shown by a previous mutagenesis study (10).

The Conserved UIM-binding Site of UbL and Ubiquitin—These shared features of the UIM-binding mode of UbL and ubiquitin raise the question of why UIM binds only weakly to monoubiquitin. The dissociation constant (K_d) defining the interaction between S5a UIM and monoubiquitin is 273 μM at pH 7 (Fig. 5*b*), and that between Hrs and monoubiquitin is 230–300 μM (16, 17). A detailed comparison of the surface of UbL and ubiquitin shows that the largest difference is a protrusion on ubiquitin caused by the bulky imidazole ring of His^{68} (Fig. 3*d*). This protrusion from the otherwise smooth ubiquitin surface may interfere with UIM binding, as can be seen in a structure of the S5a UIM-ubiquitin complex modeled by best fit superposition of the coordinates of ubiquitin to those of UbL in the lowest energy structure of the UIM-UbL complex; the imidazole of His^{68} encounters steric hindrance with the bound UIM (Fig. 3*d*). Consistent with this, substitution of the UbL residue at the same position, Val^{71}, with histidine impairs the ability of UbL to bind UIM (Table II).

To test whether the inability of monoubiquitin to bind S5a UIM is indeed due to steric hindrance, we replaced His^{68} of ubiquitin with valine, the amino acid that is found in this position in UbL and examined its effect on binding to UIM. This mutation increased the binding affinity, suggesting that the protrusion caused by His^{68} may inhibit the access of ubiquitin to UIM to some extent (Fig. 5*a*). This result suggests that the UIM-binding mode of ubiquitin is similar to that of UbL, consistent with the mutational data.

To determine whether His^{68} regulates ubiquitin binding, we examined the effect of protonation of its imidazole ring on the ability of ubiquitin to bind to UIM. The binding affinity correlated well with the pH-dependent protonation state of the His^{68} imidazole ring, as monitored by $H^{\delta 2}$ and $H^{\epsilon 1}$ chemical shifts (Fig. 5*b*). By contrast, this pH dependence was not observed for binding of the H68V mutant. Therefore, the His^{68} side chain probably has a regulatory role in the binding of ubiquitin to UIM.

We then examined whether this histidine of ubiquitin might regulate the binding of ubiquitin to UBA, another ubiquitin-binding motif that has been found in 79 human proteins (6, 9, 43). For this, we measured the binding affinity between ubiquitin and UBA from yeast Dsk2p at various pH values. It displayed a similar pH dependence to that between ubiquitin and UIM, suggesting that His^{68} of ubiquitin also regulates the binding of UBA to ubiquitin (Fig. 5*c*). This is consistent with recent structure determination of a CUE-ubiquitin complex (44). The CUE domain shows structure similarity with UBA domains and shares a common binding site on ubiquitin with UIM.

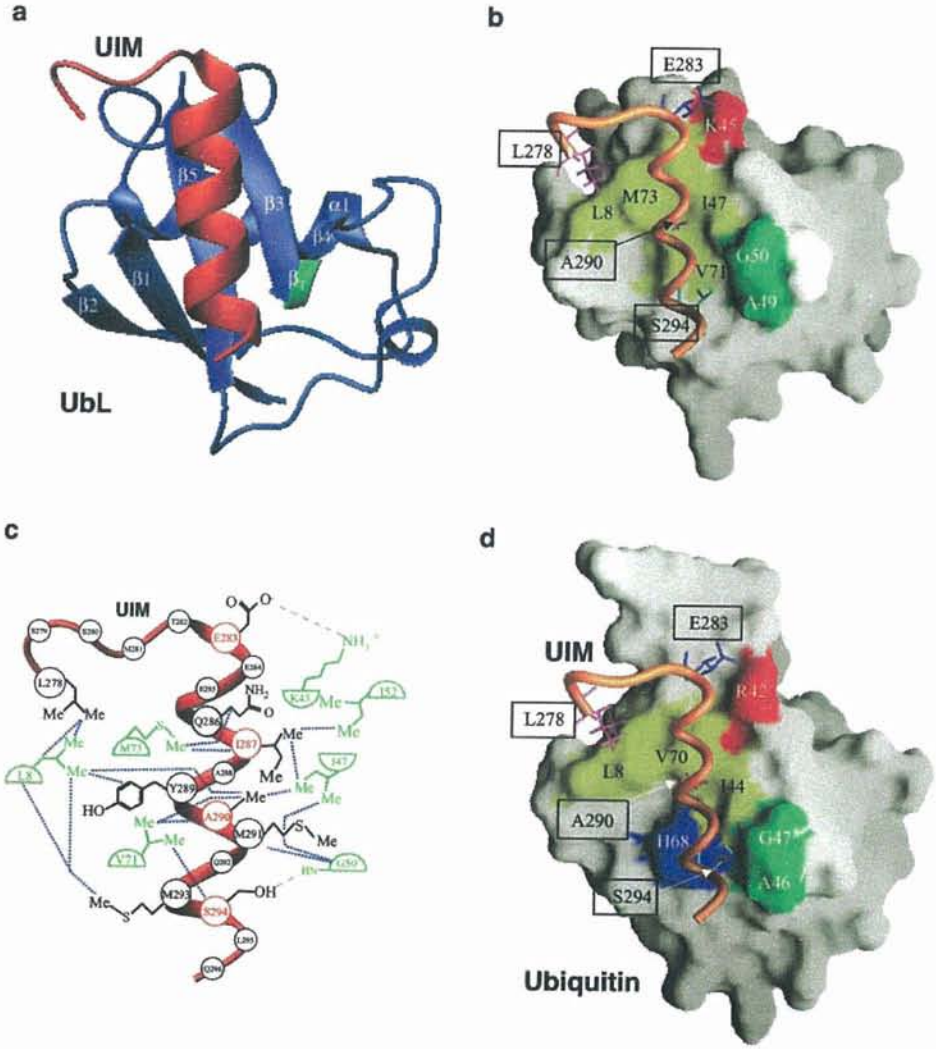

FIG. 3. **Structure of the UIM-UbL complex.** *a*, ribbon diagram of the lowest energy structure. UIM and UbL are colored *orange* and *blue*, respectively. Secondary structural elements of UbL are indicated. The Tyr^{48}-Ala^{49}-Gly^{50} segment of UbL, which forms β_T conformation, is shown in *green*. *b*, surface representation of the binding sites of UbL bound to UIM. Hydrophobic and charged residues are shown in *yellow* and *red*, respectively, and the β_T segment is shown in *green*. The side chains of UIM residues that interact with UbL are also shown. *c*, schematic diagram of the contacts between UIM and UbL. The main chain of UIM is shown in *red*. The side chains of UIM and UbL residues that form the interface are shown in *black* and *green*, respectively. Hydrophobic contacts are indicated by *blue dotted lines*, and hydrogen bonds and charged interactions are indicated by *red dashed lines*. *Me* denotes a methyl group. *d*, conserved UIM-binding sites in ubiquitin, deduced from the structure of the UIM-UbL complex, are shown on a model of the complex between human ubiquitin and UIM. Hydrophobic and charged residues are colored *yellow* and *red*, respectively, on the surface representation of human ubiquitin. The β_T segment, Phe^{45}-Ala^{46}-Gly^{47}, is shown in *green*. His^{68}, which causes the protrusion, is shown in *blue*. The model was constructed by best fit superposition of the coordinates of human ubiquitin (Protein Data Bank code 1d3z) to those of UbL in the lowest energy structure of the UIM-UbL complex.

DISCUSSION

UIM Interface of UbL—The UIM interface of UbL determined by our structure determination and mutagenesis studies is consistent with results from previous mutagenesis and chemical shift perturbation experiments of ubiquitin and UbLs (10, 16, 18, 19, 28, 29). All of those experiments suggest that the conserved hydrophobic patch composed of the side chains of Leu^8, Ile^{44}, and Val^{70} of ubiquitin is important for UIM or proteasome binding. The UIM-UbL complex reveals that the hydrophobic patch mainly functions as a pocket for the methyl group of Ala^{290}, which is conserved within UIM sequences (Fig. 1*b*) (7).

In addition to the contact mediated by the conserved hydrophobic patch, our complex structure shows that two polar interactions mediated by Glu^{283} and Ser^{294} of UIM contribute to the UIM-UbL association. Although the hydrogen bond through Ser^{294} is crucial for the binding, the electrostatic interaction between the side chains of Glu^{283} of UIM and Lys^{45} of UbL seems to be less important, because the substitution of Glu^{283} of UIM by alanine caused only a moderate effect in the binding of UIM to either UbL of HR23B or tetraubiquitin (Table II and Fig. 4). Notably, glutamic acid is well conserved at this position in UIM sequences that have been either shown or implied to bind a ubiquitin tags but not in the N-terminal UIM of human S5a or yeast S5a (Fig. 1*b*). Therefore, the weak interaction between human HR23B and the N-terminal UIM and that between yeast Rad23 and S5a may be attributed to the absence of glutamic acid at this position in their UIM sequences. Although the N-terminal UIM of human S5a binds to polyubiquitin chains much more weakly than does the C-

TABLE II
Dissociation constants

All data are the averages and estimated deviation of at least two independent measurements.

	K_d (μM)	Fold decrease
S5a UIM binding to wild type and mutant HR23B UbL		
Wild type	3.4 ± 0.3	
L8A	>1000	>300
I47A	16.6 ± 3.1	4.9
V71H	>1000	>300
M73V	1.8 ± 0.3	0.5
T75A	5.1 ± 0.7	1.5
HR23B UbL binding to wild type and mutant S5a UIM		
Wild type	3.4 ± 0.3	
L278S	15.8 ± 0.5	4.6
E283A	12.1 ± 1.0	3.6
A290S	109 ± 14	32
S294A	213 ± 24	63

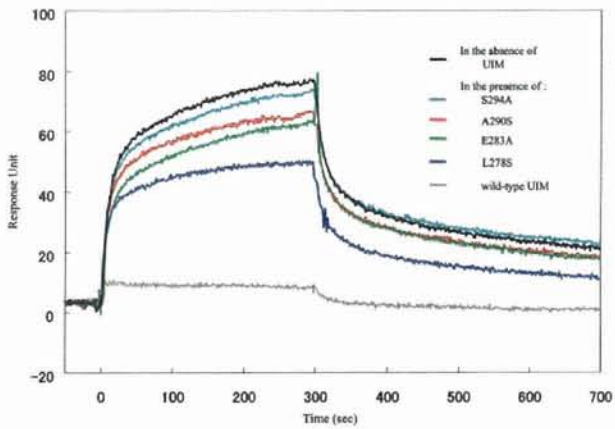

FIG. 4. **The effect of mutations on the affinity of S5a UIM for tetraubiquitin examined by a surface plasmon resonance-based competition assay.** Resonance curves were measured for 0.1 μM tetraubiquitin binding to immobilized GST-UIM in the presence or absence of 40 μM His-tagged wild type UIM or its point mutants are shown. The graph indicates that the mutants of UIM, S294A, A290S, E283A, and L278S, have weaker binding affinities for tetraubiquitin than the wild type UIM does.

terminal UIM, it still binds (10). This observation suggests that the electrostatic interaction mediated by Glu^{283} of UIM makes a nonessential contribution to the UIM-ubiquitin interaction.

The contact area of the UIM-UbL complex is 474 Å^2, as defined by the calculated change in the solvent-accessible surface area of UbL upon UIM binding. The area is comparable with the average values of 517 ± 83 and 617 ± 66 Å^2 calculated for peptide complexes of ten SH3 domains and nine SH2 domains, respectively. In the previous chemical shift perturbation experiments of the UbL domains from PLIC-2 and HR23B, NMR signals of residues close to but outside (as well as at) the interface of our UIM-HR23B complex structure also exhibited substantial changes upon binding to S5a (18 and 30). For example, the signals of Lys^{79}, Lys^{82}, Ile^{102}, and Lys^{103} of PLIC-2 exhibited substantial chemical shift perturbations upon S5a binding (18). However, the corresponding residues of the UbL domain of HR23B, Lys^{51}, Asn^{54}, Val^{74}, and Thr^{75}, make no direct contribution to the UIM interface of HR23B UbL. The noninvolvement of Thr^{75} in UIM binding was confirmed by mutagenesis; its substitution by alanine causes no apparent change in the affinity of UbL for UIM (Table II). We

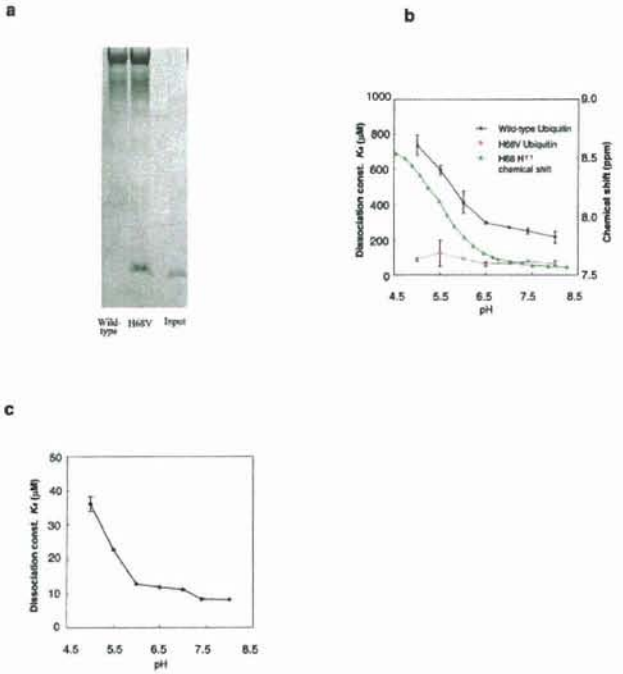

FIG. 5. **The UIM-ubiquitin interaction.** *a*, mutation of His^{68} to valine (H68V) enhances the binding affinity of ubiquitin to the UIM of S5a, shown by GST pull-down assay. The bound proteins were analyzed by GSH-mediated pull-down assay coupled with SDS-polyacrylamide gel electrophoresis and silver staining. The input lane represents 10% of the wild type ubiquitin used in the experiment. *b*, correlation between the affinity of ubiquitin for UIM and the protonation of ubiquitin His^{68}. Shown is the pH dependence of the interaction between UIM and wild type or H68V ubiquitin and the $^1H^{\varepsilon 1}$ chemical shift of His^{68} (*green*). The pK_a value of His^{68}, obtained by fitting the $H^{\varepsilon 1}$ and $H^{\delta 2}$ chemical shift data at pH range from 4.1 to 8.2, is 5.5. *c*, the pH dependence of interaction between UBA from yeast Dsk2p and ubiquitin.

assume that the NMR signals of PLIC-2 residues in the proximity of the interface were probably affected by local conformational changes or long range electrostatic effects on S5a binding. Such effects are often seen in chemical shift perturbation experiments (45) and were observed in the interaction between the UbL of HR23B and UIM (30). The UIM-UbL interaction mode proposed by based on chemical shift perturbation experiments Ryu *et al.* (30) is different from that observed in our complex structure. They assumed that residues from Glu^{283} to Gln^{296} or Gly^{297} adopts a helix, based on main chain chemical shift values of the UbL-bound UIM; that Glu^{284} and Glu^{285} of this helix locate near Lys^{48} and Lys^{51} of UbL; and that Leu 295 is positioned near the hydrophobic patch including Leu^8 of UbL. These interactions would place the helix of UIM on the UbL surface in the opposite orientation to that observed in our structure.

Role of His^{68} of Ubiquitin in UIM Binding—Our data suggest that the protonation of His^{68} of ubiquitin elicits a pH-dependent interference of the access of ubiquitin to UIM and UBA. In yeast, the substitution of this residue with alanine has been shown to lead to, albeit weak, sensitivity to cold in yeast growth (42).

The *in vivo* function of the observed pH dependence of UIM and UBA binding of ubiquitin mediated by His^{68} is unclear. Ubiquitin tags serve as a sorting signal for vesicular transport via endosomes, the *trans*-Golgi network, and multivesicular bodies (4, 46). The pH-sensitive change in their binding to downstream effectors or modulators is reminiscent of cargo adaptors that are involved in vesicular transport, such as the KDEL and mannose 6-phosphate receptors, which bind and

dissociate cargo molecules in a pH-dependent manner and thereby deliver them unidirectionally between cellular compartments at various luminal pH values (47). However, there is no evidence that ubiquitin tags move into the acidic lumenal space of vesicles. Alternatively, it may be possible that acidic membrane components affect the protonation state of this histidine in monoubiquitin tags and thus mediate their binding to UIMs of endocytic factors. Many endocytic factors with a UIM also contain ENTH, VHS, or FYVE domains that are located near the UIMs in terms of primary structure (4, 46). These domains bind to acidic lipids, such as phosphoinositides and phosphatidic acid, and thereby bring the adjacent UIMs into proximity with negatively charged membrane components, which could create a low pH environment near the membrane. Proteins, such as bacterial colicin A and pheromone-binding protein from the silk moth, are suggested to undergo conformational transitions at or near negatively charged lipid interfaces (48, 49, 50). These observations raise the intriguing possibility that His^{68} of ubiquitin may serve as a pH sensor to regulate the access of ubiquitin to UIM and UBA of downstream effectors.

His^{68} likely also regulates the conformation of Lys^{48}-linked polyubiquitin chains. The conformation of diubiquitin switches from an open to closed state as the pH increases from 4.5 to 6.8 (51). The crystal structure of diubiquitin indicates that the hydrophobic patch at the UIM interface also serves as the intersubunit interface, which includes the side chain of His^{68} (52). The same surface has been suggested to function as the intersubunit interface in the closed conformation in solution (51). Thus, the protein surface including the hydrophobic patch and His^{68} functions as the intersubunit interface of diubiquitin at higher pH but not at low pH, as occurs in ubiquitin interactions with both UIM and UBA (51). Our pH titration experiment showed that the pH dependences of the $H^{\epsilon 1}$ and $H^{\delta 2}$ chemical shifts of both subunits of diubiquitin are similar to that of monoubiquitin, shown in Fig. 5*b*, and thus the histidine side chains of diubiquitin are mostly protonated at pH 4.5 and mostly deprotonated at pH 6.8.[2] These observations raise the possibility that His^{68} is involved in regulating the intersubunit association, as well as in regulating ubiquitin-UIM and ubiquitin-UBA interactions. Notably, the same surfaces of the distal two ubiquitin subunits of tetraubiquitin function as intersubunit interfaces (51).

This histidine is conserved in the UbL domains of PLIC-2 and Parkin. A triple point mutation in the UbL domain of PLIC-2 (I75A, A77S, and H99A) abolished its binding to the proteasome (18). The mutated residues correspond to Ile^{44}, Ala^{46}, and His^{68} of ubiquitin, all of which are thought to be important for UIM binding. Therefore, the detrimental effect of the triple mutation of PLIC-2 cannot be attributed solely to substitution of the histidine.

UIM Consensus Sequence—The structure of the UIM-UbL complex, along with the binding data from the S5a UIM, UbL, and ubiquitin mutants presented here, enables us to revise the consensus sequence for ubiquitin binding by UIM. On the basis of the sequence alignment of S5a and endocytic factors (7), it was previously proposed to be ϕ-*X*-*X*-Ala-*X*-*X*-*X*-Ser-*X*-*X*-Ac, where ϕ and Ac denote a large hydrophobic residue and an acidic residue, respectively. Our data now show that, whereas Glu^{283}, Ile^{287}, Ala^{290}, and Ser^{294} of S5a contribute to UbL and ubiquitin recognition, Gly^{297}, which is located at the position of the C-terminal Ac in the proposed consensus, makes no contact with UbL and is disordered in the structure of the complex.

Residues shown to be important for UbL binding by our data are highly conserved in the UIMs of endocytic factors that have been either shown or implied to bind a ubiquitin tag (Fig. 1*b*). The most important residues, alanine and serine at positions 290 and 294 in S5a, respectively, are conserved among these factors, and a hydrophobic residue at position 287 is also well conserved. In contrast, the conservation of the acidic residue at position 283 is lower than those in UIM sequences (7). This residue seems to make a smaller contribution than the others, as revealed by our mutagenesis data (Table II and Fig. 4; see "UIM Interface of UbL"). These observations allow us to revise the consensus sequence of UIM to (Ac)-*X*-*X*-*X*-ϕ-*X*-*X*-Ala-*X*-*X*-*X*-Ser-*X*-*X*-(Ac). Fisher *et al.* (40) have also shown that glutamic acid cluster at residues 259–262 and residues Ala^{266} and Ser^{270} of Hrs UIM are important for its affinity for ubiquitin (see Fig. 1*b* for the sequence of Hrs and Ref. 37). They also showed that a mutation of Glu^{273} of Hrs UIM caused a decreased affinity, although the importance of the corresponding residue in S5a UIM, Gly^{297}, is not observed in our structure.

Conclusion—We have reported the structure of a UIM bound to a UbL. Our structural and mutational data indicate that the contact sites in UbL are highly conserved in ubiquitin, but ubiquitin also presents a histidine residue at the interface. Thus, this study provides a structural basis for the interaction between ubiquitin and UIM-containing downstream effectors. Future experiments need to be directed at establishing the functional significance of the observed pH dependence of ubiquitin binding to UIM and UBA.

Acknowledgments—We thank A. Ohno for providing the UBA domain of Dsk2p, H. Kobayashi for providing the expression plasmid for the UBA domain of Dsk2p, and K. Iwai for providing the ubiquitin-activating enzyme (E1). We thank K. Tanaka for discussion.

Addendum—After submission of this manuscript, the solution structures of the UbL of HR23A in complexed with S5a UIM (53) and the Vps27 UIM-ubiquitin complex (54) were published. The structure of HR23A UbL-UIM is similar to that of HR23B-UIM shown in this paper. The possibility of the interference of ubiquitin His^{68} for UIM binding was also discussed based on the structure. In contrast, Swanson *et al.* (54) showed that alanine substitution of His^{68} of ubiquitin impairs the binding of ubiquitin to the N-terminal UIM of Vps27.

[2] T. Tenno, unpublished data.

REFERENCES

1. Conaway, R. C., Brower, C. S., and Conaway, J. W. (2002) *Science* **296,** 1254–1258
2. Sun, Z. W., and Allis, C. D. (2002) *Nature* **418,** 104–108
3. Hoege, C., Pfander, B., Moldovan, G. L., Pyrowolakis, G., and Jentsch, S. (2002) *Nature* **419,** 135–141
4. Hicke, L. (2001) *Cell* **106,** 527–530
5. Hicke, L. (2001) *Nat. Rev. Mol. Cell. Biol.* **2,** 195–201
6. Buchberger, A. (2002) *Trends Cell Biol.* **12,** 216–221
7. Hofmann, K., and Falquet, L. (2001) *Trends Biochem. Sci.* **26,** 347–350
8. Polo, S., Sigismund, S., Faretta, M., Guidi, M., Capua, M. R., Bossi, G., Chen, H., De Camilli, P., and Di Fiore, P. P. (2002) *Nature* **416,** 451–455
9. Katzmann, D. J., Odorizzi, G., and Emr, S. D. (2002) *Nat. Rev. Mol. Cell. Biol.* **3,** 893–905
10. Young, P., Deveraux, Q., Beal, R. E., Pickart, C. M., and Rechsteiner, M. (1998) *J. Biol. Chem.* **273,** 5461–5467
11. Elsasser, S., Gali, R. R., Schwickart, M., Larsen, C. N., Leggett, D. S., Muller, B., Feng, M. T., Tubing, F., Dittmar, G. A., and Finley, D. (2002) *Nat. Cell Biol.* **4,** 725–730
12. van Nocker, S., Sadis, S., Rubin, D. M., Glickman, M., Fu, H., Coux, O., Wefes, I., Finley, D., and Vierstra, R. D. (1996) *Mol. Cell. Biol.* **16,** 6020–6028
13. Lam, Y. A., Lawson, T. G., Velayutham, M., Zweier, J. L., and Pickart, C. M. (2002) *Nature* **416,** 763–767
14. Bilodeau, P. S., Urbanowski, J. L., Winistorfer, S. C., and Piper, R. C. (2002) *Nat. Cell Biol.* **4,** 534–539
15. Shih, S. C., Katzmann, D. J., Schnell, J. D., Sutanto, M., Emr, S. D., and Hicke, L. (2002) *Nat. Cell Biol.* **4,** 389–393
16. Shekhtman, A., and Cowburn, D. (2002) *Biochem. Biophys. Res. Commun.* **296,** 1222–1227
17. Raiborg, C., Bache, K. G., Gillooly, D. J., Madshus, I. H., Stang, E., and Stenmark, H. (2002) *Nat. Cell Biol.* **4,** 394–398
18. Walters, K. J., Kleijnen, M. F., Goh, A. M., Wagner, G., and Howley, P. M. (2002) *Biochemistry* **41,** 1767–1777
19. Sakata, E., Yamaguchi, Y., Kurimoto, E., Kikuchi, J., Yokoyama, S., Yamada, S., Kawahara, H., Yokosawa, H., Hattori, N., Mizuno, Y., Tanaka, K., and Kato, K. (2003) *EMBO Rep.* **4,** 301–306
20. Tashiro, M., Okubo, S., Shimotakahara, S., Hatanaka, H., Yasuda, H., Kainosho, M., Yokoyama, S., and Shindo, H. (2003) *J. Biomol. NMR* **25,** 153–156
21. Schauber, C., Chen, L., Tongaonkar, P., Vega, I., Lambertson, D., Potts, W.,

and Madura, K. (1998) *Nature* **391,** 715–718
22. Hiyama, H., Yokoi, M., Masutani, C., Sugasawa, K., Maekawa, T., Tanaka, K., Hoeijmakers, J. H., and Hanaoka, F. (1999) *J. Biol. Chem.* **274,** 28019–28025
23. Guzder, S. N., Sung, P., Prakash, L., and Prakash, S. (1998) *J. Biol. Chem.* **273,** 31541–31546
24. Gillette, T. G., Huang, W., Russell, S. J., Reed, S. H., Johnston, S. A., and Friedberg, E. C. (2001) *Genes Dev.* **15,** 1528–1539
25. Suzuki, T., Park, H., Kwofie, M. A., and Lennarz, W. J. (2001) *J. Biol. Chem.* **276,** 21601–21607
26. van Laar, T., van der Eb, A. J., and Terleth, C. (2002) *Mutat. Res.* **499,** 53–61
27. Chen, L., and Madura, K. (2002) *Mol. Cell. Biol.* **22,** 4902–4913
28. Beal, R., Deveraux, Q., Xia, G., Rechsteiner, M., and Pickart, C. (1996) *Proc. Natl. Acad. Sci. U. S. A.* **93,** 861–866
29. Withers-Ward, E. S., Mueller, T. D., Chen, I. S., and Feigon, J. (2000) *Biochemistry* **39,** 14103–14112
30. Ryu, K. S., Lee, K. J., Bae, S. H., Kim, B. K., Kim, K. A., and Choi, B. S. (2003) *J. Biol. Chem.* **278,** 36621–36627
31. Cavanagh, J., Fairbrother, W. J., Palmer, A. G., III, and Skelton, N. J. (1996) *Protein NMR Spectroscopy*, Academic Press, San Diego, CA
32. Cornilescu, G., Delaglio, F., and Bax, A. (1999) *J. Biomol. NMR* **13,** 289–302
33. Brunger, A. T., Adams, P. D., Clore, G. M., DeLano, W. L., Gros, P., Grosse-Kunstleve, R. W., Jiang, J. S., Kuszewski, J., Nilges, M., Pannu, N. S., Read, R. J., Rice, L. M., Simonson, T., and Warren, G. L. (1998) *Acta Crystallogr. D Biol. Crystallogr.* **54,** 905–921
34. Pearlman, D. A., Case, D. A., Caldwell, J. W., Ross, W. S., Cheatham, T. E., III, DeBolt, S., Ferguson, D., Seibel, G., and Kollman, P. (1995) *Comp. Phys. Commun.* **91,** 1–41
35. Xia, B., Tsui, V., Case, D. A., Dyson, H. J., and Wright, P. E. (2002) *J. Biomol. NMR* **22,** 317–331
36. Koradi, R., Billeter, M., and Wuethrich, K. (1996) *J. Mol. Graph.* **14,** 51–55
37. Laskowski, R. A., Rullmann, J. A. C., MacArthur, M. W., Kaptein, R., and Thornton, J. M. (1996) *J. Biomol. NMR* **8,** 477–486
38. Funakoshi, M., Sasaki, T., Nishimoto, T., and Kobayashi, H. (2002) *Proc. Natl. Acad. Sci. U. S. A.* **99,** 745–750
39. Cornilescu, G., Marquardt, J. L., Ottiger, M., and Bax, A. (1998) *J. Am. Chem. Soc.* **120,** 6836–6837
40. Fisher, R. D., Wnag, B., Alam, S. L., Higginson, D. S., Robinson, H., Sundquist, W. I., and Hill, C. P. (2003) *J. Biol. Chem.* **278,** 28976–28984
41. Beal, R. E., Toscano-Cantaffa, D., Young, P., Rechsteiner, M., and Pickart, C. M. (1998) *Biochemistry* **37,** 2925–2934
42. Sloper-Mould, K. E., Jemc, J. C., Pickart, C. M., and Hicke, L. (2001) *J. Biol. Chem.* **276,** 30483–30489
43. Mueller, T. D., and Feigon, J. (2002) *J. Mol. Biol.* **319,** 1243–1255
44. Kang, R. S., Daniels, C. M., Francis, S. A., Shih, S. C., Salerno, W. J., Hicke, L., and Radhakrishnan, I. (2003) *Cell* **113,** 621–630
45. Takahashi, H., Nakanishi, T., Kami, K., Arata, Y., and Shimada, I. (2000) *Nat. Struct. Biol.* **7,** 220–223
46. Johnson, E. S. (2002) *Nat. Cell Biol.* **4,** E295–298
47. Olson, L. J., Zhang, J., Dahms, N. M., and Kim, J. J. (2002) *J. Biol. Chem.* **277,** 10156–10161
48. Merrill, A. R., Steer, B. A., Prentice, G. A., Weller, M. J., and Szabo, A. G. (1997) *Biochemistry* **36,** 6874–6884
49. van der Goot, F. G., Gonzalez-Manas, J. M., Lakey, J. H., and Pattus, F. (1991) *Nature* **354,** 408–410
50. Horst, R., Damberger, F., Luginbuhl, P., Guntert, P., Peng, G., Nikonova, L., Leal, W. S., and Wuthrich, K. (2001) *Proc. Natl. Acad. Sci. U. S. A.* **98,** 14374–14379
51. Varadan, R., Walker, O., Pickart, C., and Fushman, D. (2002) *J. Mol. Biol.* **324,** 637–647
52. Cook, W. J., Jeffrey, L. C., Carson, M., Zhijian, C., and Pickart, C. M. (1992) *J. Biol. Chem.* **267,** 16467–16471
53. Mueller, T., and Feigon, J. (2003) *EMBO J.* **22,** 4634–4645
54. Swanson, K., Kang, R. S., Stamenova, S.D., Hicke, L., and Radhakrishnan, I. (2003) *EMBO J.* **22,** 4579–4606

FEBS 28384

FEBS Letters 566 (2004) 157–161

Paramagnetic NMR study of Cu^{2+}–IDA complex localization on a protein surface and its application to elucidate long distance information

Makoto Nomura[a], Toshitatsu Kobayashi[a], Toshiyuki Kohno[b], Kenichiro Fujiwara[c], Takeshi Tenno[d], Masahiro Shirakawa[c], Itsuko Ishizaki[a], Kazuo Yamamoto[e], Toshifumi Matsuyama[e], Masaki Mishima[a], Chojiro Kojima[a,*]

[a]*Laboratory of Biophysics, Graduate School of Biological Science, Nara Institute of Science and Technology, 8916-5 Takayama, Ikoma, Nara 630-0192, Japan*
[b]*Mitsubishi Kagaku Institute of Life Sciences (MITILS), Machida, Tokyo 194-8511, Japan*
[c]*Graduate School of Integrated Science, Yokohama City University, Tsurumi, Yokohama 230-0054, Japan*
[d]*Graduate School of Science and Engineering, Ehime University, Matsuyama, Ehime 790-8577, Japan*
[e]*Division of Cytokine Signaling, Department of Molecular Microbiology and Immunology, Nagasaki University Graduate School of Biomedical Sciences, 1-12-4 Sakamoto, Nagasaki 852-8523, Japan*

Received 10 March 2004; revised 12 April 2004; accepted 13 April 2004

Available online 27 April 2004

Edited by Thomas L. James

Abstract The paramagnetic metal chelate complex Cu^{2+}-iminodiacetic acid (Cu^{2+}–IDA) was mixed with ubiquitin, a small globular protein. Quantitative analyses of ^{1}H and ^{15}N chemical shift changes and line broadenings induced by the paramagnetic effects indicated that Cu^{2+}–IDA was localized to a histidine residue (His68) on the ubiquitin surface. The distances between the backbone amide proton and the Cu^{2+} relaxation center were evaluated from the proton transverse relaxation rates enhanced by the paramagnetic effect. These correlated well with the distances calculated from the crystal structure up to 20 Å. Here, we show that a Cu^{2+}–IDA is the first paramagnetic reagent that specifically localizes to a histidine residue on the protein surface and gives the long-range distance information.

Keywords: NMR; Surface histidine; Cu^{2+}–IDA; Paramagnetic relaxation; Pseudo-contact shift; Non-metal protein

1. Introduction

In the field of biological NMR, long-range distance constraints are required for large-size multi-domain proteins and high-throughput structure determinations. Paramagnetic metals have useful properties, such as paramagnetic relaxation enhancement and pseudo-contact shift, both of which affect the NMR signals over long-range distances. For metal proteins and metal–drug–DNA complexes, these paramagnetic effects have been successfully utilized as long-range constraints in structure determinations [1–7].

Kay and co-workers [8,9] developed a method to evaluate the distance between the backbone amide proton and Cu^{2+} using the proton transverse relaxation rate enhanced by the paramagnetic effect for non-metal proteins. The method relies on localizing the paramagnetic ion to a modified target protein such as possessing a specially designed ATCUN motif tag [8,9]. Dvoretsky et al. [10] used the amide proton longitudinal relaxation rates for Mn^{2+} that was localized by mutating an amino acid of the target protein to cysteine followed by covalent modification of this residue using thiol-reactive EDTA. Both methods rely on mutation of the target protein to localize the paramagnetic metal, a procedure that may result in structural changes of the target protein.

Cu^{2+}-iminodiacetic acid (Cu^{2+}–IDA), a metal chelate complex, is an established reagent used in the area of immobilized metal ion affinity chromatography (IMAC) [11]. Immobilized Cu^{2+}–IDA on a solid support specifically binds to histidine residues ($K_d = 10^{-5}$–10^{-4} M) [11–14], and has been used to purify various protein and DNA molecules [11,15]. Other applications involving the use of Cu^{2+}–IDA IMAC have dealt with investigations concerning the structure–function relationship of proteins, which have functional histidine residues [16,17]. Although there are many applications, the precise localization of Cu^{2+}–IDA on the protein surface has not been well characterized [11,12].

Here, the localization of Cu^{2+}–IDA on three different protein surfaces was examined using chemical shift changes, line broadenings and ^{1}H transverse relaxation rate enhancements induced by the paramagnetic effects of Cu^{2+}. The proteins examined were ubiquitin, which has one histidine residue (His68) on the surface, and two other proteins that contain a C-terminal poly histidine tag, the ubiquitin-like domain of human HR23B (HR23B UbL) and the DNA binding domain of human interferon regulatory factor 4 (IRF4 DBD). The potential acquisition of long-range distance constraints was also examined.

2. Materials and methods

2.1. Sample preparation

Recombinant human ubiquitin was expressed in *Escherichia coli* BL21(DE3) as a GST-fusion protein. Following the addition of isopropyl β-D-thiogalactoside, protein expression was induced for 8 h at 30 °C in minimal medium containing ^{15}N-labeled ammonium chloride. Cells were suspended in 50 mM Tris–HCl (pH 8.0), 100 mM KCl and 1 mM Pefabloc SC (Roche). The suspension was lysed by sonication,

* Corresponding author. Fax: +81-743-72-5579.
E-mail address: kojima@bs.aist-nara.ac.jp (C. Kojima).

doi:10.1016/j.febslet.2004.04.023

ultra-centrifuged, and the supernatant was loaded onto a glutathione–Sepharose 4B column (Amersham). Elution was performed with 50 mM Tris–HCl (pH 8.0), 100 mM KCl and 30 mM glutathione. The GST–ubiquitin fraction was loaded onto a Superdex 26/60 75 pg (Amersham) gel filtration column equilibrated with 50 mM phosphate (pH 6.5), 50 mM KCl and 1 mM Pefabloc SC. The eluted GST–ubiquitin fraction was then cleaved with PreScission protease (Amersham) and loaded onto a gel filtration column. The final NMR buffer consisted of 50 mM phosphate (pH 6.7) and 200 mM KCl. The expression and purification of HR23B UbL and IRF4 DBD was performed as previously described [18].

2.2. NMR spectroscopy

The stock solution of Cu^{2+}–IDA consisted of 12.5 mM $CuCl_2$, 13.8 mM IDA, 50 mM phosphate and 200 mM KCl (pH 2.2). Following the addition of this stock solution to 0.1 or 1 mM ubiquitin, 0.1 mM HR23B UbL, and 0.5 mM IRF4 DBD, the pH of the sample solution was adjusted to pH 6.7. The ratio of Cu^{2+}–IDA/protein was 0.4 for each unless otherwise noted.

All NMR data were obtained on a Bruker DRX800 spectrometer operating at 800 MHz with a triple-resonance probe head equipped with a XYZ-gradient unit. The ^{1}H–^{15}N HSQC spectra were collected at 293 K, with 2048 (t2) times 150 (t1) complex points and spectral widths of 14 kHz (^{1}H) and 1.6 kHz (^{15}N) with carrier positions at 4.7 and 121.8 ppm, respectively. A $\pi/2$ shifted sine-bell window function was applied before zero-filling and Fourier transformation. The processing was performed using the NMRPipe package [19], while chemical shifts, linewidths and peak volumes were measured using Sparky software [20]. The transverse relaxation rates were obtained using a ^{1}H–^{15}N HSQC based spin echo experiment with a shaped refocusing pulse which was successfully used to obtain long-range distance information with the ATCUN Cu^{2+} system [8]. The relaxation delay times were 8.5, 11, 13.5, 16, 18.5, 21, 23.5, 28.5, 31, 33.5, 38.5, and 48.5 ms for Cu^{2+}–IDA–ubiquitin, and 8.5, 11, 13.5, 16, 18.5, 21, 23.5, 28.5, 33.5, 38.5, 48.5, and 68.5 ms for free ubiquitin.

2.3. Data analyses

Linewidth and chemical shift change. Linewidths were measured for 1 mM ubiquitin samples with and without 0.4 mM Cu^{2+}–IDA. The differences in linewidth were then calculated. When the Cu^{2+}–IDA–ubiquitin peak was not found compared to free ubiquitin ($S/N < 5$), the difference in linewidth was set to the maximum value of 50 Hz. Chemical shift differences of samples with and without Cu^{2+}–IDA were calculated and averaged for three independent experiments. The differences in linewidth and chemical shift values were mapped to the PDB (1UBI).

Paramagnetic ^{1}H relaxation enhancements. Three independent relaxation rate measurements of the 1 mM ubiquitin sample complexed with 0.4 mM Cu^{2+}–IDA were performed. The differences between the transverse relaxation rates with and without Cu^{2+}–IDA were calculated and averaged. The mean values of three experiments were fitted to the relation $R_{2M} = a/r^6 + b$ by non-linear fitting using Mathematica 4.2 (Wolfram) with error bar dependent weights, where R_{2M} is the transverse relaxation rate enhanced by the paramagnetic effects, r is the distance between the target proton and the relaxation center, and a and b are constants. The amide proton position was obtained from the PDB (1UBI) for the residue with the generalized order parameter $S^2 > 0.7$ [21] and the relaxation center position (assumed as Cu^{2+} atom position) was optimized.

3. Results

3.1. Localization and interaction of Cu^{2+}–IDA with ubiquitin

^{1}H–^{15}N HSQC experiments were performed in an effort to evaluate the interaction of Cu^{2+}–IDA with ubiquitin. Titration experiments using Cu^{2+}–IDA with 0.1 and 1 mM ubiquitin solutions resulted in dose-dependent and site-specific line broadenings and shifts. The localization of Cu^{2+}–IDA on the protein was not due to the presence of ionic interactions, but due to some type of coordination to the protein [16,22], since the addition of 200 mM KCl had no effect. The linewidth differences between Cu^{2+}–IDA–ubiquitin and free ubiquitin were mapped to the 3D structure of ubiquitin as shown in Fig. 1 (left), and strongly suggest that Cu^{2+}–IDA bound to ubiquitin around His68. The chemical shift differences up to 30 ppb (25 Hz) were also mapped (Fig. 1, right), supporting the presence of a specific binding site close to His68. At pH 5.0, these line broadenings and shifts were not observed even though the Cu^{2+}–IDA is stable at this pH [16,22]. This result is consistent with the notion that the imidazole nitrogen of histidine ($pK_a = 6.04$) acts as the potential electron donor for Cu^{2+}–IDA [16].

Cu^{2+} has four coordination sites. IDA can coordinate to three of these, while the protein coordinates to the remaining site [23]. Other metals such as Fe^{3+}, Co^{2+}, and Ni^{2+} can have four coordination sites, which could be chelated by IDA. ^{1}H–^{15}N HSQC spectra for these paramagnetic metal–IDA–ubiquitin complexes showed no significant line broadenings and chemical shift differences for ^{1}H, however small chemical shift differences (less than one-tenth of those for Cu^{2+}) were observed for ^{15}N around His68. This result is consistent with the notion that the localization of the paramagnetic metal–IDA complex is around His68.

3.2. Paramagnetic relaxation enhancement analysis

Transverse relaxation rates were measured using spin echo experiments based on ^{1}H–^{15}N HSQC spectra in order to obtain long-range distance information. Distances from Cu^{2+} to each amide proton were calculated using the crystal structure (PDB ID, 1UBI) and transverse relaxation rates, and were designated as the calculated and experimental distances, respectively. Using 49 out of 71 amide proton relaxation rates, the Cu^{2+} position was optimized using the Mathematica software to minimize the difference between those distances. The distances from the optimized Cu^{2+} position to N^{δ} and N^{ε} of the His68 imidazole were 5.6 ± 0.6 and 4.5 ± 1.0 Å, respectively (Fig. 2). The B-factors for N^{δ} and N^{ε} were 27 and 28

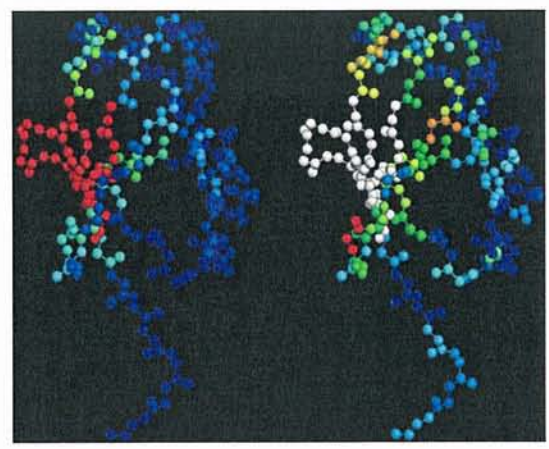

Fig. 1. Line broadenings (left) and peak shifts (right) induced by the Cu^{2+}–IDA complex mapped on the ubiquitin structure. With increasing broadenings and shifts, the color changes from blue to red. Maximum, medium and minimum values (50, 25, and 0 Hz for broadenings, and 30, 15, and 0 ppb for shifts) are colored in red, green and blue, respectively. Intermediate colors such as yellow (between green and red) are given gradually. In the peak shifts (right), white represents disappeared peaks. These pictures were drawn by RASMOL 2.6 [29].

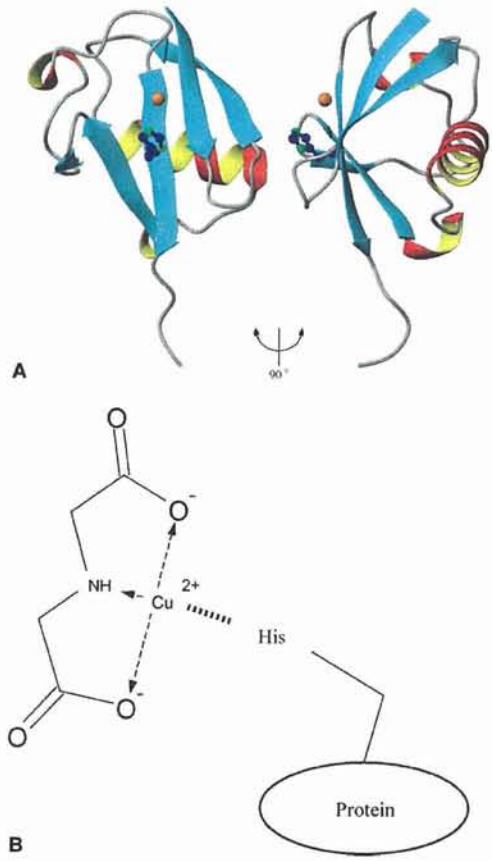

Fig. 2. The ribbon structure of ubiquitin with Cu^{2+} (A), and the chemical structure of IDA and its coordination to Cu^{2+} (B). Side chain of His68 is drawn as a ball-stick model with the two nitrogen atoms colored in green. Cu^{2+} is shown as the gold sphere. The atomic coordinate of Cu^{2+} is optimized, minimizing the calculated and observed proton transverse relaxation rates. The ribbon pictures were prepared by MOLMOL 2k.1 [30].

Å^2, respectively, and much larger than those for the backbone atoms of His68 (2–6 Å^2). This indicates that the imidazole ring is flexible and that those coordinates are less reliable. Additionally, the delocalization of the paramagnetic electron might modulate the relaxation center position [2]. Thus, it is not clear from the distance measurements if His68 does indeed bind the Cu^{2+}–IDA.

The correlation plot between the calculated and experimental distances is shown in Fig. 3. The correlation coefficient R was 0.75. The observed transverse relaxation enhancement was up to 20 Å and the mean error from the calculated values was approximately 3.6 Å. This result highlights the potential in acquiring long-range distance information using the Cu^{2+}–IDA complex, although the precision was not very high.

Relaxation experiments were repeated on samples containing a change in Cu^{2+}–IDA concentration from 0.4 to 0.2 or 0.8 mM. The relaxation data determined were fitted to the theoretical equation and were well converged. The converged coordinates of Cu^{2+} were quite similar to each other for the three data sets (RMSD = 1.3 Å). The experimental distances were correlated with the calculated ones, where $R = 0.67$ and 0.80 for the 0.2 and 0.8 mM samples, respectively.

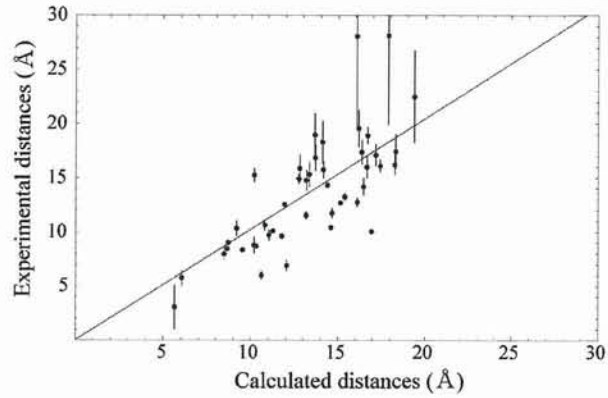

Fig. 3. Correlation plot between calculated and experimental distances from Cu^{2+} to each backbone amide proton of ubiquitin. Calculated distances were taken from the crystal structure. The experimental distances were obtained from the paramagnetic enhancement of the proton transverse relaxation rates.

4. Discussion

The binding between ubiquitin and Cu^{2+}–IDA was evaluated further by EPR. EPR spectra were recorded by a JEOL JES-TE300 X-band spectrometer at 77 K using 2.5 mM Cu^{2+}–IDA. The spectra significantly changed in the presence and absence of ubiquitin ($g_{\|} = 2.27$ and 2.32, $A_{\|} = 15.8$ and 15.9, and $g_{\perp} = 2.06$ and 2.07, respectively). In the ubiquitin titration series, Cu^{2+}–IDA spectra were explained by the weighted sum of only two spectra, i.e., free and 1:1 complex. EPR splitting patterns of Cu^{2+}–IDA complexed with a histidine were quite similar to ubiquitin complex. These data strongly suggest that Cu^{2+}–IDA coordinates to ubiquitin at one specific site, His68.

The localization of Cu^{2+}–IDA on two other proteins was investigated to reveal whether Cu^{2+}–IDA specifically binds to the surface histidine residue. The ^1H–^{15}N HSQC spectra of HR23B UbL and IRF4 DBD with and without Cu^{2+}–IDA clearly demonstrated the site-specific line broadenings and shifts around the histidine residues. Broadening ratios for all proteins examined here are given in Fig. 4. Distance information was not elucidated for HR23B UbL and IRF4 DBD, since the coordinates were not available for the free proteins. A cysteine residue is the potential binding site of Cu^{2+}–IDA, but not examined in this study because of two difficulties. First, Cu^{2+}–IDA complex cannot be used with dithiothreitol (DTT) since a Cu^{1+}-DTT complex is formed [24]. Second, a free cysteine residue decreases protein stability, and the mixture of the Cu^{2+}–IDA and a cysteine forms aggregates. Thus, *N*-ethylmaleimide was used to chemically modify the surface cysteine residue of IRF4 DBD in our experiments. Other paramagnetic metal chelate complexes, such as Mn^{2+}–NTA and Gd^{3+}–EDTA, did not bind specifically to the histidine residues for three proteins possessing a poly hisitidine tag; HR23B UbL, IRF4 DBD and the S5a UbL binding region [18]. These results are consistent with hard-soft-acid-base (HSAB) theory [25–27].

Characteristic properties of the Cu^{2+}–IDA complex, that includes highly specific localization to the histidine residue and the capability of obtaining distance information, offer clear advantages in the analysis of macromolecular intermolecular interactions such as protein–protein, protein–DNA and

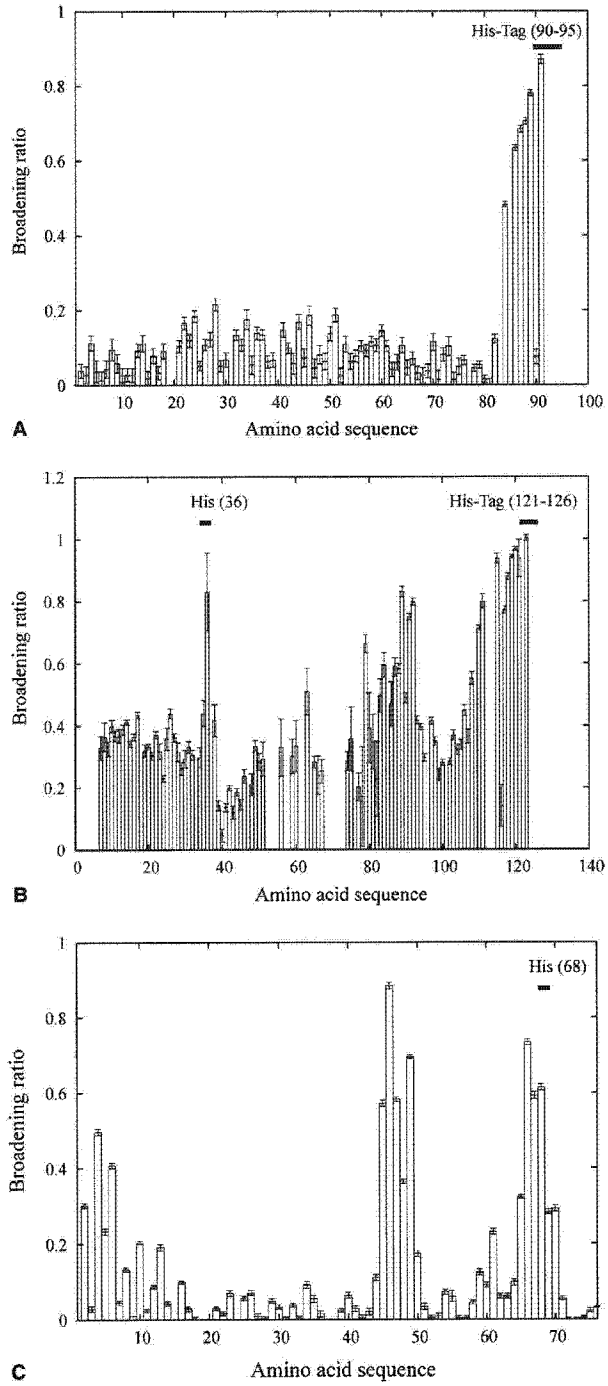

Fig. 4. The broadening ratios of HR23B UbL (A), IRF4 DBD (B), and ubiquitin (C) were plotted against the amino acid sequence. The broadening ratio is defined as $\sqrt{(I-I_0)^2}/\sqrt{I_0^2}$, where I and I_0 represent the peak height with and without Cu^{2+}–IDA (1 equiv.), respectively. The 79th to 92th residues of IRF4 DBD were spatially close to His36 in the modeled structure.

protein–ligand interactions. Hansen et al. [28] employed the paramagnetic longitudinal proton relaxation enhancement of a metal protein to detect transient intermolecular protein–protein interactions. Mal et al. [9] utilized the ATCUN Cu^{2+} system to detect protein–protein interactions. Therefore, transient interactions showing few intermolecular NOEs can be the subject of investigation using Cu^{2+}–IDA provided that a surface histidine residue is located near the interface.

Another potential application of the Cu^{2+}–IDA complex can be in the investigation of membrane proteins. Membrane proteins are usually solubilized within a detergent micelle and it is difficult to construct an expression system. Distance information in general is insufficient,and any specific modification appears daunting,to say the least. We applied the Cu^{2+}–IDA system to a membrane protein solubilized within a detergent,and the ^{1}H–^{15}N HSQC spectrum showed site-specific line broadenings and shifts (Okuda et al., unpublished results). These results indicate the potential application of the Cu^{2+}–IDA system in the study of membrane protein structures.

In conclusion, all examined paramagnetic metal chelate complexes were not localized to a specific site on the protein surface with exception of Cu^{2+}–IDA,that was specifically localized to His68 on the ubiquitin surface. This feature of Cu^{2+}–IDA was successfully utilized to elucidate long-range distance information from proton transverse relaxation enhancements. Cu^{2+}–IDA could also be used in conjunction with poly histidine tagged proteins,but it may be difficult to obtain precise distance constraints for proteins possessing many histidine residues. Application of the Cu^{2+}–IDA method to the investigation of surface histidine residues is a technique worthy of consideration, since surface histidine residues are frequently found in many proteins and can play important roles in many biochemical reactions and interactions.

Acknowledgements: We thank H. Okuda for his assistance, Prof. J.L. Markley and Prof. C. Griesinger for their critical comments, and Prof. S. Suzuki for his helpful comments on EPR analyses. This work was supported in part by Grants-in-Aid for 21st Century COE Research and Scientific Research, a Grant for the National Project on Protein Structural and Functional Analyses from MEXT (the Japanese Ministry of Education, Culture, Sports, Science and Technology), a Kaneko Narita Research Grant of Protein Research Foundation and a Grant from the Yamada Science Foundation.

References

[1] Bertini, I., Donaire, A., Jimenez, B., Luchinat, C., Parigi, G., Piccioli, M. and Poggi, L. (2001) J. Biomol. NMR 21, 85–98.
[2] Bertini, I., Luchinat, C. and Parigi, G. (2001) Solution NMR of Paramagnetic Molecules. Elsevier, Amsterdam.
[3] Bertini, I., Luchinat, C. and Piccioli, M. (2001) Methods Enzymol. 339, 314–340.
[4] Gochin, M. (1997) J. Am. Chem. Soc. 119, 3377–3378.
[5] Gochin, M. (1998) J. Biomol. NMR 12, 243–257.
[6] Kikuchi, J., Iwahara, J., Kigawa, T., Murakami, Y., Okazaki, T. and Yokoyama, S. (2002) J. Biomol. NMR 22, 333–347.
[7] Arnesano, F., Banci, L., Bertini, I., Felli, I.C., Luchinat, C. and Thompsett, A.R. (2003) J. Am. Chem. Soc. 125, 7200–7208.
[8] Donaldson, L.W., Skrynnikov, N.R., Choy, W.Y., Muhandiram, D.R., Sarkar, B., Forman-Kay, J.D. and Kay, L.E. (2001) J. Am. Chem. Soc. 123, 9843–9847.
[9] Mal, T.K., Ikura, M. and Kay, L.E. (2002) J. Am. Chem. Soc. 124, 14002–14003.
[10] Dvoretsky, A., Gaponenko, V. and Rosevear, P.R. (2002) FEBS Lett. 528, 189–192.
[11] Gaberc-Porekar, V. and Menart, V. (2001) J. Biochem. Biophys. Methods 49, 335–360.
[12] Yip, T.T., Nakagawa, Y. and Porath, J. (1989) Anal. Biochem. 183, 159–171.
[13] Hutchens, T.W. and Yip, T.T. (1990) Anal. Biochem. 191, 160–168.
[14] Mrabet, N.T. (1992) Biochemistry 31, 2690–2702.

[15] Murphy, J.C., Jewell, D.L., White, K.I., Fox, G.E. and Willson, R.C. (2003) Biotechnol. Progr. 19, 982–986.
[16] Berna, P.P., Mrabet, N.T., Van Beeumen, J., Devreese, B., Porath, J. and Vijayalakshmi, M.A. (1997) Biochemistry 36, 6896–6905.
[17] Jiang, K.Y., Pitiot, O., Anissimova, M., Adenier, H. and Vijayalakshmi, M.A. (1999) Biochim. Biophys. Acta 1433, 198–209.
[18] Fujiwara, K., Tenno, T., Sugasawa, K., Jee, J.G., Ohki, I., Kojima, C., Tochio, H., Hiroaki, H., Hanaoka, F. and Shirakawa, M. (2004) J. Biol. Chem. 279, 4760–4767.
[19] Delaglio, F., Grzesiek, S., Vuister, G.W., Zhu, G., Pfeifer, J. and Bax, A. (1995) J. Biomol. NMR 6, 277–293.
[20] Goddard, T.D. and Kneller, D.G. (1999) Sparky 3. University of California, San Francisco.
[21] Schneider, D.M., Dellwo, M.J. and Wand, A.J. (1992) Biochemistry 31, 3645–3652.
[22] Sulkowski, E. (1987) in: Protein Purification: Micro to Macro (Burgess, R.R., Ed.), pp. 149–162, Alan R. Liss Inc, New York.
[23] Hochuli, E., Dobeli, H. and Schacher, A. (1987) J. Chromatogr. 411, 177–184.
[24] Kr zel, A., Lesniak, W., Jezowska-Bojczuk, M., Mlynarz, P., Brasun, J., Kozlowski, H. and Bal, W. (2001) J. Inorg. Biochem. 84, 77–88.
[25] Aime, S., D'Amelio, N., Fragai, M., Lee, Y.M., Luchinat, C., Terreno, E. and Valensin, G. (2002) J. Biol. Inorg. Chem. 7, 617–622.
[26] Kemple, M.D., Ray, B.D., Lipkowitz, K.B., Prendergast, F.G. and Nageswara Rao, B.D. (1988) J. Am. Chem. Soc. 110, 8275–8787.
[27] Petros, A.M., Mueller, L. and Kopple, K.D. (1990) Biochemistry 29, 10041–10048.
[28] Hansen, D.F., Hass, M.A., Christensen, H.M., Ulstrup, J. and Led, J.J. (2003) J. Am. Chem. Soc. 125, 6858–6859.
[29] Sayle, R.A. and Milner-White, E.J. (1995) Trends Biochem. Sci. 20, 374.
[30] Koradi, R., Billeter, M. and Wuthrich, K. (1996) J. Mol. Graph. 14, 51–55, 29–32.

Nucleic Acids Symposium Series No. 48 105-106

Solution NMR study of DNA recognition mechanism of IRF4 protein

Itsuko Ishizaki[1], Makoto Nomura[1], Kazuo Yamamoto[2], Toshifumi Matsuyama[2], Masaki Mishima[1] and Chojiro Kojima[1]

[1]Laboratory of Biophysics, Graduate School of Biological Science, Nara Institute of Science and Technology, 8916-5 Takayama, Ikoma, Nara 630-0192, Japan and [2]Division of Cytokine Signaling, Department of Molecular Microbiology and Immunology, Nagasaki University Graduate School of Biomedical Science, 1-12-4 Sakamoto, Nagasaki 852-8523, Japan

ABSTRACT

Transcription factor IRF-4 prefers the DNA sequence including CCGAAA. The consensus sequence of the IRF family proteins is NNGAAA, and all crystal structures indicate the NN region does not interact with IRF proteins directly. Here the sequence preference of IRF-4 was investigated by NMR and fluorescence anisotropy as an example of the indirect sequence recognition. The ^{1}H-^{15}N HSQC spectra of the IRF-4/DNA complex containing the CCGAAA sequence indicated that the 1:1 complex was formed. The dissociation constants (K_d) for two DNA oligomers containing CCGAAA and GGGAAA were determined by fluorescence anisotropy, but their difference was very small.

INTRODUCTION

IRF-4 is a lymphoid and myeloid restricted member of the IRF transcriptional family.[1,2] PU.1/IRF-4/DNA ternary complex has been cocrystallized and analyzed biochemically,[3] however, PU.1 is not related to many physiological functions of IRF-4.[2,4-7] Recognition sequences of IRF-4 have been determined (Yoshida *et al.*, personal communication) using the selected and amplified binding sequences (SAAB) method.[8] Most of them contain the CCGAAA sequences, though the consensus sequence of IRF family proteins is known as NNGAAA. In the crystal structures of IRF/DNA complexes including the PU.1/IRF-4/DNA ternary complex (GTGAAA), NN sequence does not have direct contacts with IRF family proteins. In this study, we have investigated the sequence preference of IRF-4 physicochemically using heteronuclear two-dimensional NMR and fluorescence anisotropy.

MATERIALS AND METHODS

Recombinant human IRF-4 DNA binding domain (20-137) was expressed in *Escherichia coli* BL21(DE3) strain with minimal medium containing ^{15}N-labeled ammonium chloride. All DNA oligomers were purchased from Fasmac Corp. (Atsugi, Japan). All NMR spectra were measured using a Bruker DRX800 NMR spectrometer operating at 800 MHz. The K_d values were determined by the fluorescence anisotropy measurement using Beacon 2000 (Pan Vera Corp., Madison) with oligonucleotides labeled with hexachlorofluorescein. The K_d values were calculated from the fluorescence anisotropy data using Prism 3.0 software (GraphPad, San Diego).

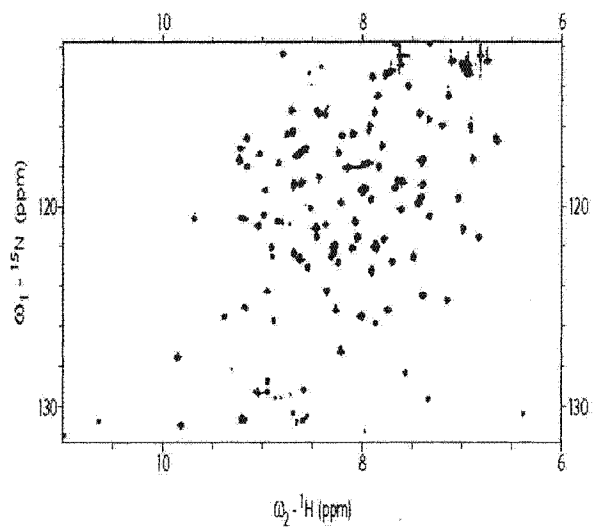

Figure 1. ^{1}H-^{15}N HSQC spectrum of the IRF-4/DNA complex recorded by 800 MHz NMR at 30 °C. DNA oligomer containing CCGAAA sequence was used. The 0.2 mM NMR sample contains 50 mM sodium phosphate (pH 6.7), 100 mM sodium chloride, 0.1 mM EDTA and 1 mM DTT.

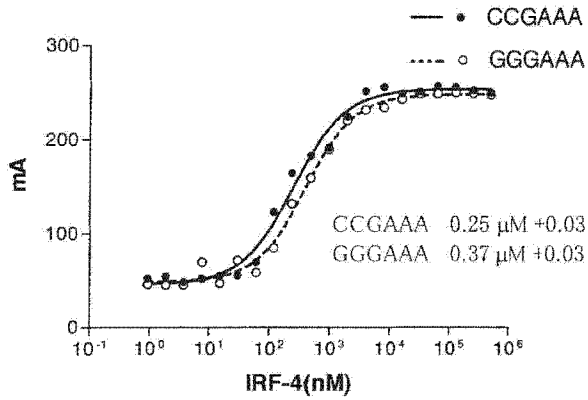

Figure 2. Florescence anisotropy of the fluorescein-labeled DNA with different concentration of IRF-4 recorded by Beacon 2000 at 22 °C. Filled and open circles show the data for the DNA oligomers containing CCGAAA and GGGAAA sequences, and the solid and dotted lines are best fitted to calculate K_d values, respectively. The sample contains 10 nM DNA with 25 mM sodium phosphate buffer (pH 6.5) and 1 mM DTT. Protein concentration is changed from 1 nM to 0.5 mM.

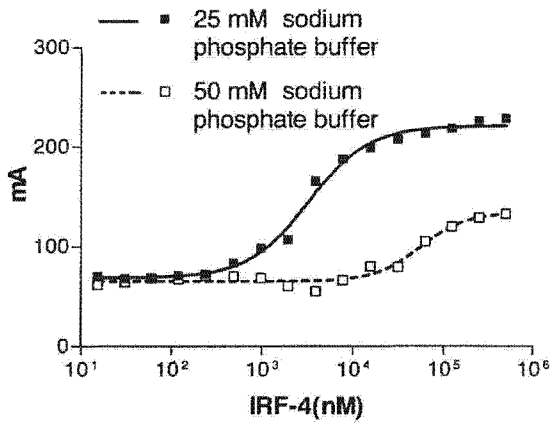

Figure 3. Salt concentration dependence of the IRF-4/DNA complex formation. The measurement condition was same to figure 2. Filled and open squares show the data for 25 mM and 50 mM sodium phosphate buffer, respectively. The solid line is identical to that shown in Figure 2.

RESULT AND DISCUSSION

The DNA oligomer containing the CCGAAA sequence was titrated to the ^{15}N enriched IRF-4 DNA binding domain, and both the ^{1}H-^{15}N HSQC spectra and the imino proton spectra were recorded. Changing the ratio of IRF-4 to DNA from 1:0 to 1:1, the spectra changed drastically. In Figure 1, the ^{1}H-^{15}N HSQC spectrum of IRF-4/DNA complex is shown. The spectra recorded at the ratio 1:1 and 1:2 were similar each other, and no significant shift was detected. Thus the DNA oligomer containing the CCGAAA sequence forms the 1:1 complex with IRF-4.

To evaluate the affinity of IRF-4 to two DNA sequences containing CCGAAA and GGGAAA, Kd values were determined by the fluorescent anisotropy measurement (Figure 2). The determined K_d values were 0.25 μM and 0.37 μM for the CCGAAA and GGGAAA sequences, respectively. This difference was very small, but larger than the experimental error. The increase of the salt concentration attenuates the affinity significantly (Figure 3). NOESY spectra of two DNA sequences containing CCGAAA and GGGAAA showed that they were the canonical B form conformation and no special feature was found. These results indicate the difference of two DNA oligomers including the CCGAAA and GGGAAA sequence is very small at both free and complex states. Thus the small difference of the indirect recognition site, such as DNA dynamics, may reflect the sequence preference of IRF-4 drastically. The detailed calorimetric study may solve this question.

REFERENCES

1. Mamane, Y., Sharma, S., Grandvaux, N., Hernandez, E. and Hiscott, J. (2002) *Annu. Rev. J. Interferon Cytokine Res.* **22**, 135-143.

2. Maracki, S. and Fenton, M. J. (2002) *Annu. Rev. J. Interferon Cytokine Res.* **22**, 121-133.

3. Escalante, C. R., Brass, A. L., Pongbala, J. M. R., Shatova, E., Shen, L., Singh, H. and Aggarwal, A. K. (2002) *Mol. Cell* **10**, 1097-1105.

4. Gupta, S. Jiang, M., Anthony, A. and Pernis, A.B. (1999) *J. Exp. Med.* **190**, 1837-1848.

5. Yamagata, T., Nishida, J., Tanaka, T., Sakai, R., Mitani, K., Yoshida, M., Taniguti, T., Yazaki, Y. and Hirai, H. (1996) *Mol. Cell. Biol.* **16**, 1283-1294.

6. Marecki, S. Atchison, M. L. and Fenton, M. J. (1999) *J. Immunol.* **163**, 2713-2722.

7. Nelson, N., Marks, M. S., Driggers, P. H. and Ozato, K. (1993) *Mol. Cell. Biol.* **13**, 588-599.

8. Blackwell, T. K., Kretzner, L., Blackwood, E. M., Eisenman, R. N. and Weintraub, H. (1990) *Science* **250**, 1149-1151.

Journal of Biomolecular NMR (2005) 31: 269–270
DOI 10.1007/s10858-005-0522-0

Letter to the Editor: ^{1}H, ^{15}N and ^{13}C backbone and side-chain assignments of the rice phytochrome B PAS1 domain and backbone assignments of the PAS1-PAS2 domain

Toshitatsu Kobayashi[a], Masaki Mishima[a], Kayo Akagi[b], Nobuya Sakai[b], Etsuko Katoh[b], Makoto Takano[b], Toshimasa Yamazaki[b] & Chojiro Kojima[a,*]
[a]*Graduate School of Biological Sciences, Nara Institute of Science and Technology (NAIST), 8916-5, Takayama, Ikoma, Nara, 630-0192, Japan;* [b]*2-1-2 Kan-non-dai, National Institute of Agrobiological Sciences, Tsukuba, 305-8602, Japan*

Received 08 November 2004; Accepted 23 December 2004

Key words: PAS, photomorphogenesis, phyB C-terminal, red/far-red light photoreceptor, rice

Biological context

Phytochromes consist of a family of red/far-red light photoreceptors in plants that regulate photomorphogenic events ranging from seed germination and deetiolation, to the induction of flowering (Neff et al., 2000). Following absorption of red light, phytochromes translocate from the cytoplasm to the nucleus, and subsequently regulate gene expression through interactions with transcription factors such as basic-helix-loop-helix proteins (Quail, 2002). Phytochrome proteins possess two major structural domains, the N- and C- terminal domains (Quail, 1997). The N-terminal domain (~74 kDa) possesses a covalently attached linear tetrapyrrole chromophore (phytochromobilin) and is sufficient for light absorption and photoreversibility. The C-terminal domain (~55 kDa), which plays a role in phytochrome dimerization and downstream signaling, consists of two PAS (PER-ARNT-SIM) domains and one histidine kinase-like domain. The PAS domains are a family of sensor protein domains involved in signal transduction in a wide range of organisms (Taylor and Zhulin, 1999). With phytochromes, a loss of function missense mutation cluster was located within the PAS domains, suggesting that these domains are crucial for phytochrome signaling (Quail et al., 1995; Ni et al., 1998; Chen et al., 2003; Matsushita et al., 2003). In an effort to delineate the mechanism underlying photomorphogenesis in plants, it is important to investigate the three- dimensional structure and dynamic aspects of this domain. The assignment of the rice phytochrome B PAS domains presented here represents the first step toward the study of phytochrome signaling using NMR.

Methods and experiments

The rice phytochrome B (phyB) PAS1 and PAS1-PAS2 domains (residues 666-782 and 666-923, respectively) were cloned into the pET32c expression vector (Novagen) and over-produced in *E. coli* BL21 (DE3) RIL (Novagen) as thioredoxin and hexa-histidine fusion proteins. $^{13}C/^{15}N$- or ^{15}N-labeled protein was induced by the presence of 1 mM IPTG at 25 °C in M9 minimal medium containing $^{15}NH_4Cl$ and [U–^{13}C] glucose or unlabeled glucose, respectively. Cells obtained from M9 cultures were lysed by sonication. The lysate was centrifuged and the supernatant was loaded onto a Ni-NTA agarose resin (Qiagen). Proteins were eluted with imidazole in a stepwise manner. The sample fraction was then passed through a Superdex 26/60 75 pg gel filtration column (Amersham). Following removal of the fused tag by enterokinase (Novagen) was performed, Hi-trap Q anion-exchange (Amersham) and Superdex 26/60 75 pg columns were used to further purify the samples. The identity and integrity of the protein samples was confirmed by N-terminal sequencing, MALDI/TOF MS and SDS-PAGE.

All NMR measurements were carried out on a Bruker AV500 spectrometer equipped with a $^{1}H/^{13}C/^{15}N$ cryogenic probe and a DRX800 spectrometer

*To whom correspondence should be addressed. E-mail: kojima@bs.naist.jp

equipped with a $^{1}H/^{13}C/^{15}N/^{31}P$ probe at 30 °C. The PAS1 and PAS1-PAS2 domains were dissolved in 90%/10% H_2O/D_2O containing 50 mM phosphate (pH 6.8), 20 mM KCl and 5 mM DTT at a protein concentration of 0.8 mM and 0.2 mM, respectively. For the PAS1 domain, the backbone and side-chain resonances were obtained from the following spectra: HNCACB, HN(CO)CACB, HN(CA)CO, HNCO, C(CO)NH, H(CCO)NH, 4D-HC(CO)NH, HCCH-TOCSY, ^{15}N-edited TOCSY-HSQC and 2D-NOESY experiments. For the sequential backbone assignments of the PAS1-PAS2 domain, HNCACB, HN(CO)CACB, HN(CA)CO and HNCO were recorded. The NMR data were processed using NMRPipe (Delaglio et al., 1995) and analyzed using SPARKY (T. D. Goddard and D. G. Kneller, SPARKY 3, University of California, San Francisco).

Extent of assignments and data deposition

Supplementary Figure 1a and 1b show the $^{1}H/^{15}N$ HSQC spectra of the phyB PAS1 and phyB PAS1-PAS2 domains, respectively. The phyB PAS1 domain consists of 124 residues including 7 N-terminal residues originating from the vector, while the phyB PAS1-PAS2 domain consists of 261 residues including 3 residues from the vector. For the backbone atoms of the PAS1 domain, 97.5, 97.5, 97.5, 97.3 and 98.4% of the ^{1}HN, ^{15}N, $^{13}C_{\alpha}$, $^{13}C_{\beta}$ and $^{13}C'$ resonance assignments were obtained, respectively. For the aliphatic and aromatic side-chain atoms of the PAS1 domain, 92.7% of the ^{1}H and ^{13}C resonance assignments were obtained. For the PAS1-PAS2 domain, 98.4, 98.4, 98.9, 99.2 and 98.9% of the ^{1}HN, ^{15}N, $^{13}C_{\alpha}$, $^{13}C_{\beta}$ and $^{13}C'$ backbone resonance assignments were obtained. The L695-T696, L698, V709, I713-F714, K740-Q748 and K750-I756 in the PAS1 domain, and the V709, I713, T743-Q748, K750-G751 and V755 in the PAS1-PAS2 domain showed minor peaks. The chemical shift assignments (^{1}H, ^{15}N, ^{13}C) of the rice phyB PAS1 and PAS1-PAS2 domains have been deposited in the BioMagResBank (http://www.bmrb.wisc.edu) under accession number 6439 and 6440, respectively.

Acknowledgements

We thank Ryo Tabata for help in the early part of this work and Junko Tsukamoto for technical support in performing the N-terminal sequencing and MALDI/TOF MS analyses. This work was supported in part by Grants-in-Aid for Scientific Research and 21st Century COE Research from MEXT (the Ministry of Education, Culture, Sports, Science and Technology) of Japan, and a grant from the Ministry of Agriculture, Forestry and Fisheries of Japan (Rice Genome Project, PR-4101).

Supplementary material to this paper is available in electronic form at: http://dx.doi.org/10.1007/s10858-005-0522-0.

References

Chen, M., Schwab, R. and Chory, J. (2003) *Proc. Natl. Acad. Sci. USA.*, **24**, 14493–14498.
Delaglio, F., Grzesiek, S., Vuister, G.W., Zhu, G., Pfeifer, J. and Bax, A. (1995) *J. Biomol. NMR.*, **6**, 277–293.
Neff, M.M., Fankhauser, C. and Chory, J. (2000) *Genes Dev.*, **14**, 257–271.
Ni, M., Tepperman, J.M. and Quail, P.H. (1998) *Cell*, **95**, 657–667.
Matsushita, T., Mochizuki, N. and Nagatani, A. (2003) *Nature*, **424**, 571–574.
Quail, P.H., Boylan, M.T., Parks, B.M., Short, T.W., Xu, Y. and Wagner, D. (1995) *Science*, **268**, 675–680.
Quail, P.H. (1997) *Plant Cell Environ.*, **20**, 657–665.
Quail, P.H. (2002) *Nat. Rev. Mol. Cell Biol.*, **3**, 85–93.
Taylor, B.L. and Zhulin, B. (1999) *Microbiol. Mol. Biol. Rev.*, **63**, 479–506.

Linker Region of a Halobacterial Transducer Protein Interacts Directly with Its Sensor Retinal Protein†

Yuki Sudo,‡,§ Hideyasu Okuda,§ Masaki Yamabi,‡ Yuta Fukuzaki,§ Masaki Mishima,§ Naoki Kamo,‡ and Chojiro Kojima*,§

Laboratory of Biophysical Chemistry, Graduate School of Pharmaceutical Sciences, Hokkaido University, Sapporo 060-0812, Japan, and Laboratory of Biophysics, Graduate School of Biological Sciences, Nara Institute of Science and Technology, 8916-5 Takayama, Ikoma, Nara 630-0192, Japan

Received November 18, 2004; Revised Manuscript Received January 25, 2005

ABSTRACT: *p*HtrII, a *pharaonis* halobacterial transducer protein, possesses two transmembrane helices and forms a signaling complex with *pharaonis* phoborhodopsin (*p*pR, also called *pharaonis* sensory rhodopsin II, NpSRII) within the halobacterial membrane. This complex transmits a light signal to the sensory system located in the cytoplasm. It has been suggested that the linker region connecting the transmembrane region and the methylation region of *p*HtrII is important for binding to *p*pR and subsequent photosignal transduction. In this study, we present evidence to suggest that the linker region itself interacts directly with *p*pR in addition to the interaction in the membrane region. An *in vitro* pull-down assay revealed that the linker region bound to *p*pR, and its dissociation constant (K_D) was estimated to be approximately 10 μM using isothermal titration calorimetry (ITC). Solution NMR analyses showed that *p*pR interacted with the linker region of *p*HtrII (*p*HtrII$^{G83-Q149}$) and resulted in the broadening of many peaks, indicating structural changes within this region. These results suggest that the *p*HtrII linker region interacts directly with *p*pR. There was no demonstrable interaction between the C-terminal region of *p*pR (*p*pR$^{Gly224-His247}$) and either the linker region (*p*HtrII$^{G83-Q149}$) or the transmembrane region (*p*HtrII$^{M1-E114}$) of *p*HtrII. On the basis of the NMR, CD, and photochemical data, we discuss the structural changes and role of the linker region of *p*HtrII in relation to photosignal transduction.

The *pharaonis* halobacterial transducer protein, *p*HtrII, from *Natronomonas (Natronobacterium) pharaonis* (*1*), is a two-transmembrane helical protein and belongs to a family of two-transmembrane helical methyl-accepting chemotaxis proteins (MCPs) (*2*−*4*). MCPs exist as homodimers composed of a ~50−60-kDa subunit and form the ternary complex with CheA and CheW. Chemical stimuli activate phosphorylation cascades that modulate flagella motors (*5*). In relation to chemoreception in bacteria, MCPs act not only as transducers but also as signal receptors. In terms of photoreception in *Natronomonas pharaonis*, a direct interaction is required between *p*HtrII and the photosignal receptor *pharaonis* phoborhodopsin (*p*pR,[1] also called *pharaonis* sensory rhodopsin II, NpsRII) (*1*, *6*). *p*pR transmits light signals to *p*HtrII through changes resulting from the interaction, and *p*HtrII eventually activates phosphorylation cascades that modulate flagella motors. The active (signaling) intermediates of the *p*pR/*p*HtrII complex are referred to as the M and O intermediates (*7*). Using these sensing systems, *N. pharaonis* avoids harmful near-UV light (λ < 520 nm).

*p*pR is a member of the seven-transmembrane helical retinal group of proteins (*8*) that includes rhodopsin (*9*), bacteriorhodopsin (*10*), and others (*11*, *12*). *p*pR and *p*HtrII are stable within the membrane and *n*-dodecyl-β-D-maltoside micelles (*13*, *14*). Expression systems utilizing *Escherichia coli* cells can provide large amounts of *p*pR and *p*HtrII proteins (several mg/L culture) (*15*). Consequently, *p*pR and *p*HtrII have been well-characterized over the past few years using various methods (for reviews, see refs *1*, *8*, *16*, and *17*). Sudo et al. demonstrated a 2:2 stoichiometry in the *p*pR/*p*HtrII complex (*18*) and calculated the binding constant between *p*pR and *p*HtrII under various conditions (*19*, *20*). Figure 1 shows the crystal structure of the *p*pR/*p*HtrII complex (*21*). Of particular importance is the hydrogen-bonding network between Tyr199^{ppR} and Asn74^{pHtrII} and between Thr189^{ppR} and Glu43^{pHtrII}/Ser62^{pHtrII} and the phenolic ring of Tyr199^{ppR} and Phe28^{pHtrII} (*14*, *22*). Furthermore, the importance of Thr189^{ppR}, Asp193^{ppR}, and Thr204^{ppR} for the interaction has also been examined (Yamabi et al., manuscript in preparation).

*p*HtrII is composed of four regions consisting of two-transmembrane segments (TM1 and TM2), a linker region, a methylation region, and a signaling domain. Kim et al. reported on the X-ray structure of the methylation region and the signaling region of a serine chemotaxis receptor (Tsr)

† This work was supported by grants from Japanese Ministry of Education, Culture, Sports, Science, and Technology.

* To whom correspondence should be addressed. Telephone: 81-743-72-5571. Fax: 81-743-72-5579. E-mail: kojima@bs.naist.jp.

‡ Hokkaido University.

§ Nara Institute of Science and Technology.

[1] Abbreviations: *p*pR, *pharaonis* phoborhodopsin; *p*HtrII, *pharaonis* halobacterial transducer II; DM, *n*-dodecyl-β-D-maltoside; OG, *n*-octyl-β-D-glucoside; NMR, nuclear magnetic resonance; ITC, isothermal titration calorimetry; K_D, dissociation constant; GST, glutathione-*S*-transferase; CD, circular dichroism; HSQC, heteronuclear single-quantum correlation; TM, transmembrane segment; *p*HtrII$^{G83-Q149}$, *p*HtrII fragment from Gly83 to Gln149.

10.1021/bi047573z CCC: $30.25
Published on Web 03/26/2005

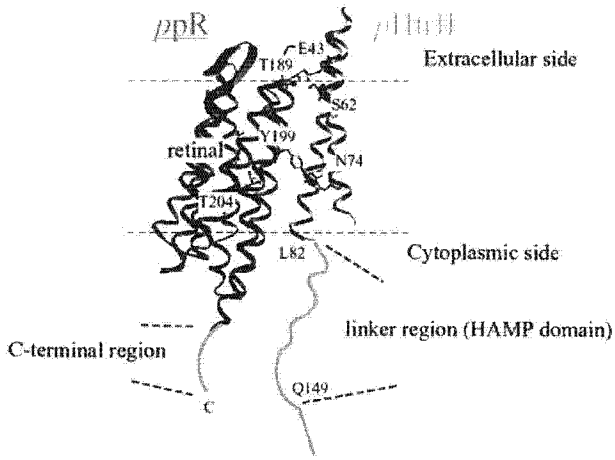

FIGURE 1: X-ray crystallographic structure of the *p*pR/*p*HtrII complex. The structure was obtained from the Protein Data Bank (PDB code 1H2S). *p*pR and *p*HtrII form the signaling complex in the dark and photolyzed state. Light stimulation activates *p*pR and triggers trans−cis photoisomerization of the retinal chromophore. Relaxation of the retinal leads to the functional processes during the photocycle. *p*pR transmits light signals to *p*HtrII in the membrane. *p*HtrII forms a ternary complex with CheA and CheW and activates phosphorylation cascades that modulate flagella motors. In this paper, the *p*HtrII linker region and the C-terminal region of *p*pR were designated as the regions from *p*HtrII^{Leu83} to *p*HtrII^{Gln149} and from *p*pR^{Gly224} to *p*pR^{His247}, respectively. The membrane normal is roughly in the vertical plane of this figure, and the top and bottom regions correspond to the extracellular and cytoplasmic sides, respectively.

(*23*). The X-ray structure of the transmembrane region of *p*HtrII in the *p*pR/*p*HtrII complex has recently been reported (*21*) (Figure 1). Tsr belongs to the two-transmembrane helical MCPs (*2*, *24*). Although these results have facilitated the next stage of research to do with photosignal transduction, detailed structural investigations concerning the linker region connecting the membrane region and the methylation region of MCPs have not been reported. The linker region posesses what is referred to as a HAMP domain, which is typically found in various proteins such as histidine kinases, adenylyl cyclases, methyl-accepting chemotaxis/phototaxis proteins, and phosphatases (*2*, *24*). This domain plays crucial roles in the phosphorylation or methylation of homodimeric receptors by transmitting conformational changes from the periplasmic to the cytoplasmic domain. It has been suggested that the linker region of the transducer may participate in the interaction with the sensor retinal pigment because certain residues within the linker region of HtrI (the *Halobacterium salinarum* transducer protein) modulate the sensory rhodopsin (sR, also called sensory rhodopsin I, sRI) photocycle (*4*, *25*). Umemura et al. reported that the sensing of cytoplasmic pH by chemoreceptors involves the linker region (*26*). Recently, Yang et al. reported that the E−F loop of *p*pR was located near the part of the *p*HtrII linker region based on probe accessibility data, disulfide formation assays, the flash photolysis analysis, as well as the FRET analysis (*27*). In this paper, we demonstrate that the linker region of *p*HtrII (*p*HtrII$^{G83-Q149}$) interacts directly with *p*pR.

MATERIALS AND METHODS

Protein Expression and Purification. The *p*pRHis (His refers to a hexa-histidine tag at the C terminus) expression plasmid was constructed as previously described (*28*). The GST-*p*HtrII$^{G83-Q149}$ gene was prepared by employing a PCR methodology. Primer 5′-GGATCCTGGGCGGTGACAC-CGCCGCCTCGCTTTC-3′ (the underlined bases indicate the added restriction site for *Bam*HI) and the reverse primer 5′-TTATGTGCCTGCTCTGCGTCCTCGCGAGCGTTC-3′ (the underlined bases indicate the added stop codon) were designed for the PCR. The PCR product was subcloned into the pGEM-T Easy (Promega) plasmid vector. The *Bam*HI and *Eco*RI digested fragment was ligated to a pGEX5X-3 vector (Amarsham). This cloning strategy resulted in the following N- and C-terminal peptide sequence: GST-*p*HtrII^{83}GGDTA- - -AEQAQ^{149}.

*p*pR was expressed in *E. coli* strain BL21 (DE3) (Invitrogen, Carlsbad, CA) at 37 °C in 2× YT medium containing ampicillin and subsequently induced by the addition of 1 mM IPTG and 10 μM all-*trans* retinal. Preparation of crude membranes and purification of *p*pR was performed as previously described (*29*). GST-*p*HtrII$^{G83-Q149}$ and GST only were overexpressed in *E. coli* strain BL21 (DE3) star cells (Invitrogen, Carlsbad, CA) and subsequently induced by the addition of 1 mM IPTG (Wako Pure Chemical Industries, Osaka, Japan). *p*pR proteins possessing a histidine tag at the C terminus were solubilized with 1.0% *n*-dodecyl-β-D-maltoside (DM) and subsequently purified using a Ni column as previously described (*29*).

IPTG-induced cells that expressed GST alone and GST-*p*HtrII linker were harvested by centrifugation at 4 °C. Pellets were resuspended in buffer A [50 mM Tris-HCl (pH 8.0) and 5 mM $MgCl_2$] and then broken by sonication. The supernatants were collected by ultracentrifugation (140000*g* for 30 min at 4 °C) to remove the membrane fraction. GST and GST-*p*HtrII$^{83-149}$ were then applied to a glutathione sepharose 4B resin column. The resin was washed extensively with buffer B [50 mM Tris-HCl (pH 8.0) and 300 mM NaCl] to remove nonspecifically bound proteins. GST and GST-tagged *p*HtrII were then eluted with buffer C [50 mM Tris-HCl (pH 8.0), 300 mM NaCl, and 10 mM glutathione]. The sample medium was exchanged by Amicon Ultra (Millipore, Bedford, MA) filtration and the samples were finally suspended in a buffer solution containing 150 mM NaCl, 50 mM Tris-HCl (pH 7.5), and 1 mM $CaCl_2$. Purified GST-*p*HtrII$^{83-149}$ was incubated with Factor Xa (0.5 unit/mg of protein) for ~3−4 h at 4 °C. The reaction was stopped by the addition of a protease inhibitor (1,5-dansyl-Glu-Gly-Arg-chloromethyl ketone dihydrochloride, Calbiochem). GST-digested *p*HtrII$^{G83-Q149}$ was separated by gel-filtration chromatography in a buffer solution containing 150 mM NaCl, 50 mM Tris-HCl (pH 7.5), and 1 mM $CaCl_2$. A final yield of 30 mg of *p*HtrII$^{83-149}$/L of cell culture was obtained.

Uniformly ^{15}N-single-labeled and ^{15}N-,^{13}C-double-labeled proteins for NMR experiments were prepared by growing the cells in standard minimal medium containing 0.5 g/L ^{15}N-ammonium chloride (Isotec Inc., Miamisburg, OH) or ^{15}N-ammonium chloride and 1.0 g/L ^{13}C-D-glucose (Isotec Inc., Miamisburg, OH). Transformed cells were initially grown at 37 °C in 1 mL of LB medium and were inoculated directly into 200 mL of isotope-labeled standard minimal M9 medium followed by inoculation in 4 L of labeled medium.

Binding Assay between the pHtrII Linker Region (pHtrII$^{G83-Q149}$) and ppR. GST-tagged *p*HtrII$^{G83-Q149}$, GST-digested *p*HtrII$^{G83-Q149}$, and *pp*R were concentrated by Amicon Ultra (Millipore, Bedford, MA) filtration. Buffer solutions were exchanged completely by dialysis against a buffer solution [300 mM NaCl, 10 mM Tris-HCl (pH 8.0), and 1% OG] for 1 week using a 3-kDa cutoff dialysis cassette (Molecular cut off, 3000, Daiichi Pure Chemicals Co. Ltd. Tokyo, Japan). The protein concentration of *pp*R and *p*HtrII was determined using the molar extinction coefficient at 500 nm (40 000 M^{-1} cm^{-1}) (*30*) and 280 nm (Tyr (1420 M^{-1} cm^{-1}), respectively.

An *in vitro* pull-down assay was performed using a glutathione sepharose column essentially as previously described (*18*, *31*). Purified *p*HtrII$^{G83-Q149}$ (300 μM) and *pp*R (30 μM) were mixed in a molar ratio of 1:10 in buffer B containing 1% OG and then incubated for 1 h at room temperature with gentle stirring. After the mixed samples were bound to the glutathione sepharose resin, the resin was poured into a chromatography column and washed extensively with buffer B (about 5-fold volume against the column volume) to remove nonspecifically bound proteins. Bound *pp*R was eluted with buffer C.

For the isothermal titration calorimetry (ITC) experiments, the *pp*R and *p*HtrII$^{G83-Q149}$ sample buffer solutions were exchanged completely by dialysis against a buffer solution [150 mM NaCl, 10 mM Tris-HCl (pH 8.0), and 0.05% DM] for 1 week using a 3-kDa cutoff dialysis cassette. The protein concentration of *pp*R and *p*HtrII was 0.35 and 0.03 mM, respectively. All ITC experiments were performed at 308 K on a VP-ITC Micro Calorimeter (Microcal Inc). For control experiments, DM-containing buffers were used to ensure that there was no effect because of the detergent. The binding parameters were estimated using the following binding scheme:

$$ppR/pHtrII_n \leftrightarrow ppR + npHtrII$$

where *n* represents the number of *p*HtrII molecules required for the formation of a complex with *pp*R. Data were evaluated by employing the Origin-ITC software package.

Flash Photolysis with or without pHtrII$^{G83-Q149}$. The apparatus and procedure for flash spectroscopy was essentially as previously described (*32*). The decay rate of the M photointermediate of the wild-type *pp*R (20 μM) with or without *p*HtrII$^{G83-Q149}$ (80 μM) and *p*HtrII$^{M1-L159}$ (80 μM) was observed at 350 nm. Truncated *p*HtrII expressed from position 1−159 was used instead of the whole protein because the truncated transducer tightly interacts with *pp*R [K_D = 0.1 μM (in the dark state)] (*22*). The temperature was maintained at 20 °C.

NMR Spectroscopy. NMR experiments for $^{13}C/^{15}N$-labeled *p*HtrII$^{G83-Q149}$ were performed at 283 K on a Bruker Avance 500 spectrometer with a ^1H [$^{13}C/^{15}N$] pulse field gradient cryogenic probe in a buffer solution containing 50 mM KCl and 50 mM KP_i (pH 6.5) without detergent. NMR experiments for $^{13}C/^{15}N$-labeled *pp*R were performed at 303 K on a Bruker Avance 500 spectrometer in a buffer solution containing 50 mM KCl, 10 mM citric acid (pH 5.0), and 3% 1,2-dihexanoyl-*sn*-glycero-3-phosphocholine (DHPC) as a detergent. The protein concentration was 1.8 and 0.4 mM for *p*HtrII and *pp*R, respectively. The assignments of the ^1H, ^{13}C, and ^{15}N resonances of *p*HtrII$^{G83-Q149}$ and *pp*R were obtained using ^1H-^{15}N HSQC and a series of triple-resonance experiments: HN(CO)CACB, HNCACB, HNCO, HN(CA)-CO, and (H)N(CO-TOCSY)NH incorporating pulsed field gradients, water flip-back pulses, and a sensitivity enhancement scheme. All data were processed using NMRPipe (*33*) and analyzed using Sparky (http://www.cgl.ucsf.edu/home/sparky/) (*34*). The NMR experiments for $^{13}C/^{15}N$-labeled *p*HtrII$^{G83-Q149}$ in the presence of *n*-octyl-β-D-glucoside (OG) were performed at 283 K on a Bruker Avance 500 MHz spectrometer in a buffer solution containg 50 mM KCl and 50 mM KP_i (pH 6.5).

CD Spectroscopy. The CD spectrum was recorded on a JASCO (Tokyo, Japan) J-720W CD spectropolarimeter. The CD spectrum was recorded between 260 and 200 nm (0.1 cm cell) at 0.1 nm intervals with a scan speed of 20 nm/min. Signals were averaged over 6 separate scans. The protein concentration was 20 μM in a buffer solution containing 50 mM KP_i, 50 mM KCl, and OG (free, 0.5, 1.0, and 7.2%).

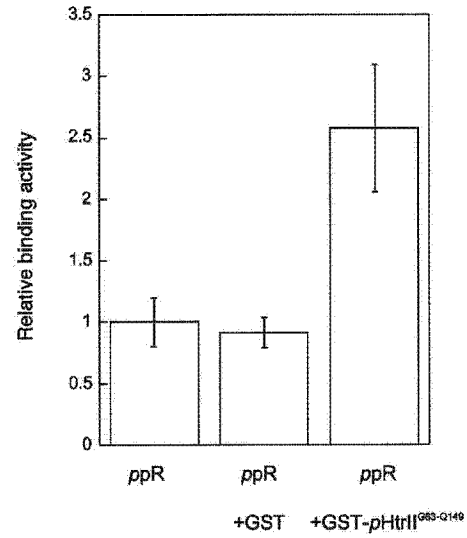

FIGURE 2: *In vitro* pull-down assay using glutathione sepharose resin. *pp*R was applied to the column without GST and GST-*p*HtrII$^{G83-Q149}$ (lane 1), with GST (lane 2), and with GST-*p*HtrII$^{G83-Q149}$ (lane 3). After the column was washed extensively with buffer B (for details, see the Materials and Methods) to remove nonspecifically bound proteins, bound proteins were eluted with buffer C (see the Materials and Methods). The eluted material was collected, and the UV−vis spectrum of *pp*R (λ_{max} = 500) was then measured.

RESULTS

Direct Interaction between the pHtrII Linker Region and ppR. In an effort to determine whether the *p*HtrII linker region (*p*HtrII$^{G83-Q149}$) interacts with *pp*R, we performed the *in vitro* pull-down assay (see the Materials and Methods and refs *18* and *31*). *pp*R adsorbed onto the glutathione sepharose 4B resin containing immobilized GST-*p*HtrII$^{G83-Q149}$. Figure 2 shows the adsorbed fraction of *pp*R in the presence of GST (lane 2) and in the absence or presence of GST-*p*HtrII$^{G83-Q149}$ (lanes 1 and 3, respectively). Specifically adsorbed *pp*R was detected in the presence of GST-*p*HtrII$^{G83-Q149}$.

The interaction between the *p*HtrII linker region (*p*HtrII$^{G83-Q149}$) and *pp*R was then quantitatively examined

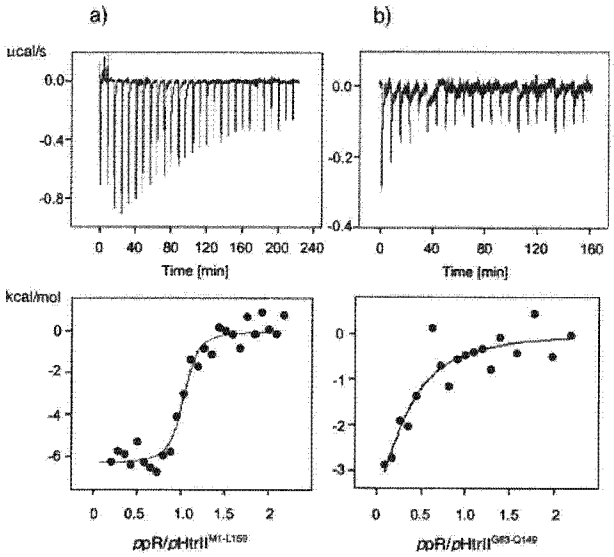

FIGURE 3: Isothermal calorimetric titration curves of *p*pR titrated with *p*HtrII$^{M1-L159}$ (a) and *p*HtrII$^{G83-Q149}$ (b). The upper panels represent the raw data. The lower panels represent the enthalpy changes per mole plotted as a function of the molar ratio of *p*pR to *p*HtrII. The solid lines represent best-fit curves (for details, see the Materials and Methods). The dilution heat of *p*pR is subtracted in these calculations. The binding parameters determined are listed in Table 1.

using ITC. Figure 3 shows the titration curves of *p*pR with *p*HtrII$^{M1-L159}$ and *p*HtrII$^{G83-Q149}$. Our ITC experiments were performed under the conditions established by Engelhard and co-workers (*22*). In these experiments, *p*HtrII$^{M1-L159}$ and *p*HtrII$^{G83-Q149}$ were maintained at 318 and 308 K, respectively, and *p*pR was added in increments of 10 μL using a syringe. The dissociation constant of *p*HtrII$^{M1-L159}$ (0.10 μM) was similar to the previously reported value (0.16 μM) (*22*). The dissociation constant (K_D) of *p*HtrII$^{G83-Q149}$ (10 μM) increased by nearly two orders and was almost identical to that of the signaling complex (*p*pR$_M$/*p*HtrII) (15 μM), as determined by flash photolysis (*18*). Our ITC results and those of other researchers are summarized in Table 1.

Table 1: Dissociation Constants (K_D) of Various *p*pR/*p*HtrII Mutant Complexes for the Ground State of *p*pR as Determined by ITC

	temperature (K)	pH	K_D (μM)	reference
*p*HtrII$^{M1-T157}$	318	8	0.16	*a*
*p*HtrII$^{M1-E114}$	318	8	0.23	*a*
*p*HtrII$^{M1-L159}$	318	8	0.1	this paper
*p*HtrII$^{G83-Q149}$	308	8	10	this paper
*p*HtrII$^{M1-L159}$ (interaction with *p*pR$_M$)	293	7.2	15	*b*

[a] Data from Hippler-Mreyen et al. (*22*). [b] Data from Sudo et al. (*18*).

From these binding assays, we concluded that the *p*HtrII linker region (*p*HtrII$^{G83-Q149}$) was able to interact directly with *p*pR in the dark state. Thus, the transmembrane and linker regions of *p*HtrII are both important in facilitating a direct and tight interaction with *p*pR.

Detailed Analysis of the Interaction between the pHtrII Linker Region and ppR by Solution NMR Spectroscopy. Solution NMR spectroscopy was performed in an effort to analyze the details of the *p*HtrII$^{G83-Q149}$–*p*pR interaction. Figure 4 shows a ^{1}H-^{15}N HSQC NMR spectrum of 1.8 mM *p*HtrII$^{G83-Q149}$ in 50 mM KP$_i$ (pH 6.5) and 50 mM KCl at

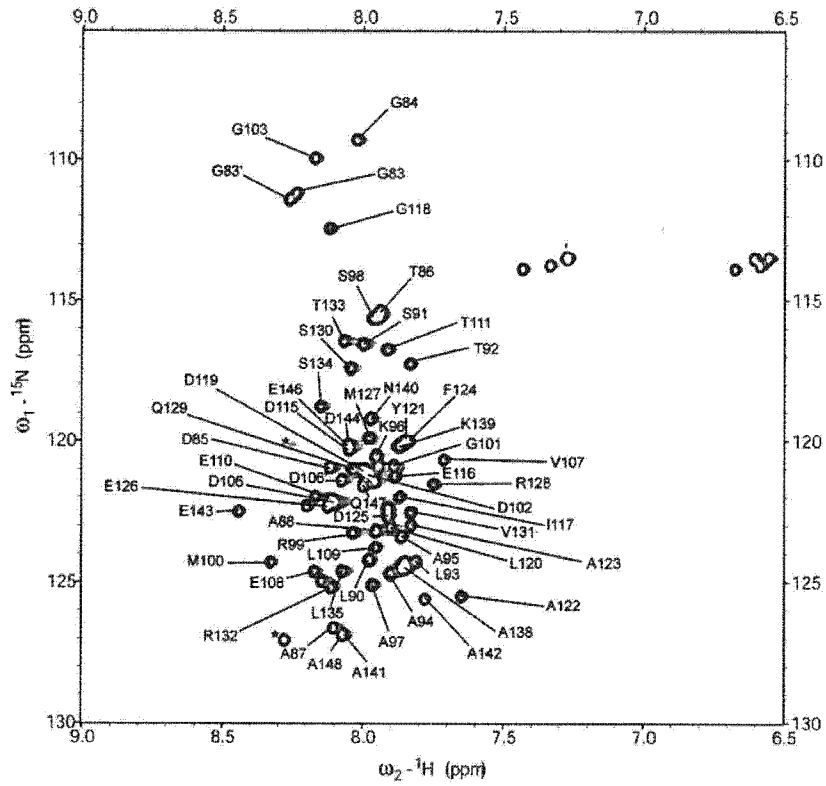

FIGURE 4: Two-dimensional ^{1}H-^{15}N HSQC spectrum of *p*HtrII$^{G83-Q149}$. The spectrum was recorded in 50 mM KCl and 50 mM KP$_i$ (pH 6.5) at 283 K on a 500 MHz NMR spectrometer. The assignments of the backbone amide protons are labeled.

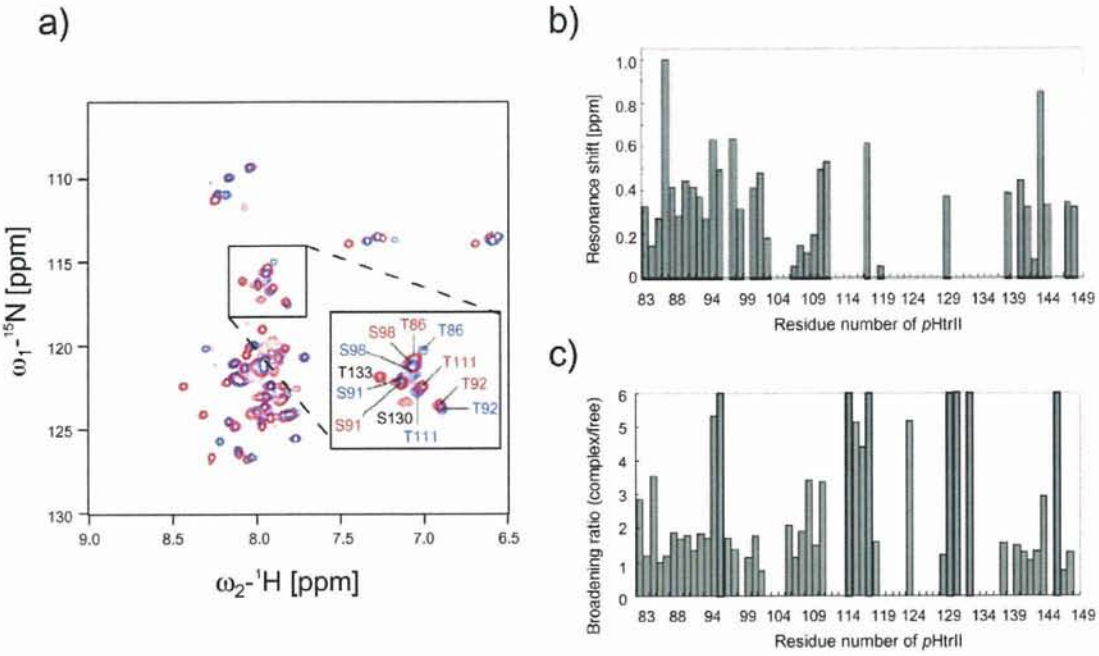

FIGURE 5: (a) Two-dimensional ^{1}H-^{15}N HSQC spectra of *p*HtrII$^{G83-Q149}$ with (blue) or without (red) *p*pR. Both spectra were recorded in 50 mM KP_i (pH 6.5) and 50 mM KCl at 283 K with 1% OG. (b and c) *p*pR-induced chemical-shift changes and the broadening ratios (complex/free ^{1}H line width), respectively, of the amide cross-peaks of *p*HtrII$^{G83-Q149}$.

283 K without detergent. Almost all of the signals from the backbone amide groups were observed. Backbone ^{1}H, ^{13}C, and ^{15}N resonances of 60 residues were assigned using conventional triple-resonance techniques, resulting in identification of the random structure based on ^{13}C chemical shifts. The assigned resonances are labeled in the figure. The ^{1}H-^{15}N HSQC spectra of 0.25 mM *p*HtrII$^{G83-Q149}$ in 50 mM KP_i (pH 6.5) and 50 mM KCl at 283 K with 1% OG as a detergent in the absence or presence of *p*pR (0.25 mM) are shown in Figure 5a as red and blue, respectively. *p*pR-induced resonance shifts and broadening were detected for many peakes, indicating that *p*HtrII$^{G83-Q149}$ interacts with *p*pR. This result is consistent with results of the aforementioned binding assays (Figures 2 and 3). Parts b and c of Figure 5 show the amino acid residues of *p*HtrII$^{G83-Q149}$ that showed resonance shifts and broadening, respectively, induced following association with *p*pR. The broadening of the resonance peaks originated from the middle part of the linker region (*p*HtrII$^{E114-R132}$), indicating that some structural changes in this region may occur.

Effect of the C-Terminal Region of ppR on the Interaction with the pHtrII Linker Region. The interaction between *p*pR and the *p*HtrII linker region (*p*HtrII$^{G83-Q149}$) was examined using stable isotope-labeled *p*pR (not *p*HtrII). Figure 6a shows a ^{1}H-^{15}N two-dimensional NMR spectrum of 0.4 mM *p*pR in 10 mM citric acid (pH 5.0) and 50 mM KCl at 303 K. Backbone ^{1}H, ^{13}C, and ^{15}N resonances of 23 residues in the C-terminal region of *p*pR (Figure 6b) were assigned using a conventional triple-resonance procedure. The assigned resonances are labeled in the figure. The ^{1}H-^{15}N HSQC spectra of 0.20 and 0.3 mM *p*pR in the absence or presence of 0.20 mM *p*HtrII$^{G83-Q149}$ and 0.3 mM of *p*HtrII$^{M1-E114}$ are shown in parts d and c of Figure 6, respectively. *p*HtrII-induced resonance shifts and broadening were not detected. Thus, the C-terminal region of *p*pR (*p*pR$^{Gly224-His247}$) does not participate in the interaction with *p*HtrII within the detergent micelles.

Does pHtrII Linker Region Interact with the M Photointermediate of ppR? Sudo et al. estimated the K_D value of the complex between the M intermediate of *p*pR (*p*pR$_M$) and *p*HtrII$^{M1-L159}$ (*18*). In an effort to determine whether this linker region (*p*HtrII$^{G83-Q149}$) can interact with *p*pR$_M$, a photochemical assay (see the Materials and Methods and refs *19* and *20*) was employed. Figure 7 shows the decay of the M photointermediate of *p*pR in the presence or absence of *p*HtrII. The decays of *p*pR$_M$ with or without *p*HtrII$^{M1-L159}$ are shown as gray lines, reproduced from ref *18*, and that of *p*pR$_M$ with *p*HtrII$^{G83-Q149}$ is shown as black dots. The molecular ratios of both *p*pR/*p*HtrII$^{M1-L159}$ and *p*HtrII$^{G83-Q149}$ were 1:10. The decay rate constant of the M photointermediate of *p*pR in the absence or presence of *p*HtrII$^{M1-L159}$, as well as that in the presence of *p*HtrII$^{G83-Q149}$, was 1.66, 0.82, and 1.69 s^{-1}, respectively. No significant change in the M decay rate was observed when *p*HtrII$^{83-149}$ was added to a molar ratio of *p*pR/*p*HtrII$^{G83-Q149}$ = 1:30 (data not shown). When *p*pR interacts with *p*HtrII$^{M1-L159}$, the decay rate of the M photointermediate of *p*pR changes ~2−4-fold. Thus, *p*HtrII$^{G83-Q149}$ does not interact with *p*pR$_M$, although the fragment might still physically interact but possibly not sufficiently to alter the decay rate.

DISCUSSION

Hippler-Mreyen et al. reported that the dissociation constant of *p*HtrII$^{M1-T157}$ (0.16 μM) was nearly 3 orders smaller than the value of *p*HtrII^{M1-L82} (>100 μM) (*22*). *p*HtrII^{M1-L82} lacks the linker region of *p*HtrII. They concluded that *p*HtrII$^{G83-T157}$ is important for the interaction with *p*pR. Yang et al. made use of the fluorescence resonance energy

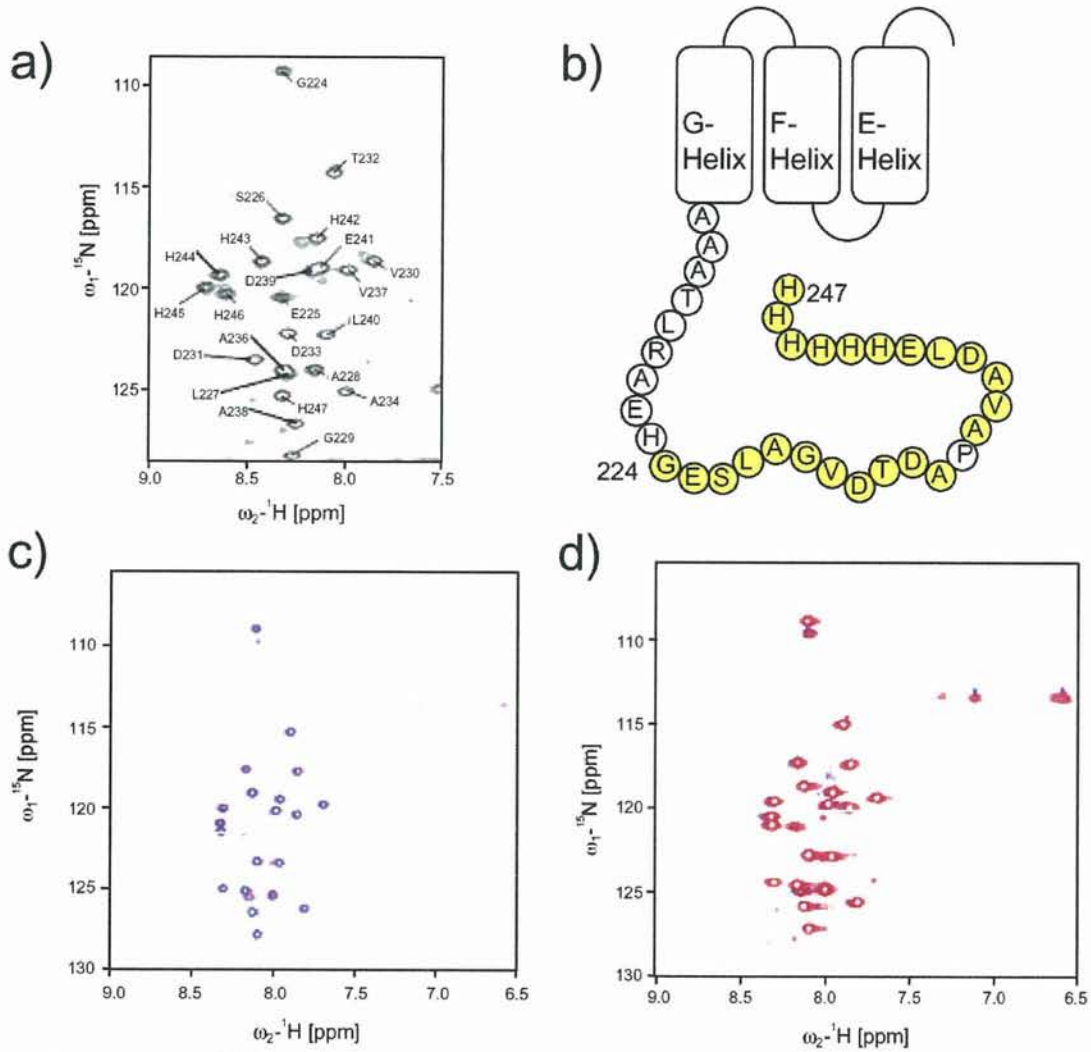

FIGURE 6: (a) Two-dimensional ^{1}H-^{15}N HSQC spectrum of *p*pR. The spectrum was recorded in 50 mM KCl and 50 mM KP_i (pH 6.5) at 283 K on a 500 MHz NMR spectrometer. The assignments of the backbone amide protons are labeled. (b) 23 residues located in the C-terminal region of *p*pR that were assigned. (c and d) ^{1}H-^{15}N HSQC spectra of the ^{15}N-labeled *p*pR in the absence (red) or presence (blue) of *p*HtrII$^{G83-Q149}$ (c) and *p*HtrII$^{M1-E114}$ (d).

transfer (FRET) method and concluded that the interaction site of *p*pR with the linker region is located near Ser-154 (*27*). From mutation analyses, Spudich and co-workers reported that *p*HtrII^{Gly83} and *p*HtrII^{Ala88} are important residues involved in photosignal transduction (*35*). In this paper, we demonstrated that the *p*HtrII linker region interacted directly with *p*pR. Our results are consistent with their data. Thus, the *p*HtrII linker region is important in facilitating a direct interaction with *p*pR that eventually results in phototransduction by the *p*pR/*p*HtrII complex.

OG was used as a detergent in the solution NMR analyses because *p*pR was not stable in the detergent-free solution. However, OG may affect the structure of the *p*HtrII linker region. From the CD spectroscopic measurements, it was determined that the secondary structure of the linker region changed from a random to an α-helical structure following the addition of OG. The cmc of the detergent (about 1%) is critical in determining the formation of the α helix (Figure 8a). This result is consistent with NMR experiments where the addition of OG altered the ^{1}H-^{15}N HSQC spectra in a manner dependent on the micelle concentration of OG (Figure 8b). Additionally, the resonance shifts and broadening were mainly detected in two short regions, the N-terminal and C-terminal parts of the *p*HtrII linker region, suggesting the formation of two α helices. These results suggest that the linker region would act as the chameleon sequence. Formation of an α helix is consistent with the data presented by Danielson et al., where the linker region of Tar corresponding to the *p*HtrII linker region forms an α helix by the cysteine and disulfide bond scanning method (*36*).

The nature of the OG-induced resonance shifts and broadening related to the *p*HtrII linker region was clearly different from those of the *p*pR-induced spectral changes (see Figures 5 and 8). These results reflect the presence of a specific interaction between the *p*HtrII linker region and *p*pR and that the observations made were not derived from detergent-induced changes. *p*pR-induced chemical-shift changes of the *p*HtrII signals mainly occurred in the N-terminal part of the *p*HtrII linker region spanning about 20 residues, suggesting that this N-terminal region possesses specific binding sites for *p*pR.